Journal of Photochemistry and Photobiology C: Photochemistry Reviews 15 (2013) 53–72

Contents lists available at SciVerse ScienceDirect

Journal of Photochemistry and Photobiology C: Photochemistry Reviews

journal homepage: www.elsevier.com/locate/jphotochemrev

Invited review

Nanomaterials formulations for photothermal and photodynamic therapy of cancer

Edakkattuparambil Sidharth Shibu[a], Morihiko Hamada[a], Norio Murase[a], Vasudevanpillai Biju[a,b,*]

[a] Health Research Institute, National Institute of Advanced Industrial Science and Technology (AIST), Takamatsu, Kagawa 761-0395, Japan
[b] PRESTO, Japan Science and Technology Agency, Tokyo 332-0012, Japan

ARTICLE INFO

Article history:
Received 27 July 2012
Received in revised form
19 September 2012
Accepted 26 September 2012
Available online 23 October 2012

Keywords:
Phototherapy
Photothermal therapy
Photodynamic therapy
Cancer
Surface plasmon
Singlet oxygen
Nanoparticles

ABSTRACT

Nanomaterials with well-defined size, shape, composition, and surface functionalities offer multimodal and multifunctional platforms for various bioanalytical, bioimaging, and therapeutic applications. In this review, we focus on the different theranostic formulations of nanomaterials based on gold, silver, silica, semiconductor quantum dots, upconversion lanthanides, oxide magnets, polymers, liposomes, carbon nanotubes, graphene and carbon nanohorns, and their applications in photothermal and photodynamic therapy of cancer.

© 2012 Elsevier B.V. All rights reserved.

Contents

Abbreviations: DPBF, 1,3-diphenylisobenzofuran; ADPA, 9,10-anthracenedipropionic acid; RGD, arginine–glycine–aspartic acid; CTAB, cetyltrimethyl ammonium bromide; cw, continuous wave; Cy, cyanine dyes; EGFR, epidermal growth factor receptor; GNPs, gold nanoparticles; GNRs, gold nanorods; GNS, gold nanoshells; GSNPs, gold-shelled silica nanoparticles; GO, graphene oxide; HNPs, hyaluronic acid nanoparticles; MWCNT, multi-walled carbon nanotubes; MTGNPs, multiple twinned gold nanoparticles; NPs, nanoparticles; NIR, near infra red; OCT, optical coherence tomography; PDT, photodynamic therapy; PS, photosensitizer; PTT, photothermal therapy; PAA, poly acrylic acid; PEG, poly ethylene glycol; PLA, poly lactic acid; PSGNPs, popcorn-shaped gold nanoparticles; PI, propidium iodide; QDs, quantum dots; ROI, reactive oxygen intermediates; RGO, reduced graphene oxide; AgNTs, silver nanotriangles; SWCNT, single-walled carbon nanotube; $^1O_2$, singlet oxygen; SERS, surface enhanced Raman scattering; SPR, surface plasmon resonance; SET, surface-energy transfer; $^3O_2$, triplet oxygen; UCL, upconversion luminescence.

* Corresponding author at: Health Research Institute, National Institute of Advanced Industrial Science and Technology (AIST), Takamatsu, Kagawa 761-0395, Japan.
E-mail address: v.biju@aist.go.jp (V. Biju).

1389-5567/$20.00 © 2012 Elsevier B.V. All rights reserved.
http://dx.doi.org/10.1016/j.jphotochemrev.2012.09.004

Edakkattuparambil Sidharth Shibu received his Under Graduate (2002) and Mater (2004) Degrees in Chemistry from the University of Calicut. Subsequently, he joined the Department of Chemistry at Indian Institute of Technology (IIT) Madras for his graduate studies, where he obtained a PhD degree in Chemistry (2011) under the guidance of Prof. T. Pradeep. In January 2011, he joined AIST as a Postdoctoral Fellow under the supervision of Prof. V. Biju. Since November 2011, he is a JSPS Postdoctoral Fellow working in AIST with Prof. Biju. His current research is focused on the synthesis of multimodal nanomaterials and investigations of their applications for bioimaging and phototherapy. He is the recipient of the best paper awards of Taiwan's RCAS-TNNA Symposium and JSPS-DST Japan-India Bilateral Seminar.

Morihiko Hamada obtained his Undergraduate (2009) and Master (2011) degrees in Engineering from Kagawa University in Japan. Since April 2012 he is a graduate student affiliated with AIST Innovation School and Kagawa University. He is carrying out his graduate research in AIST under the guidance of Prof. V. Biju (AIST) and Prof. Shunsuke Nakanishi (Kagawa University). His graduate research is on the development of unidirectional energy donor-acceptor systems and investigation of Förster Resonance Energy Transfer in the systems. He is the recipient of the international travel award of NEC and the Nippon Electronic Corporation (NEC) and the award of the Chugoku-Shikoku Branch of the Chemical Society of Japan (2012).

Norio Murase received his master degree in Chemistry from Tokyo University. Subsequently he entered into Hitachi Ltd. for the study of materials for high density optical memory, for which he obtained a PhD there in 1994. Immediately after that, he gave up the position in Hitachi, and joined in National Institute of Advanced Industrial Science and Technology (AIST). He is currently the group leader of Nanobioanalysis Research Group, Health Research Institute, AIST. Since 2010, he is also appointed as a Visiting Professor at Kwansei Gakuin University, Japan. His current research is focused on the development of silica encapsulated quantum dots.

Vasudevanpillai Biju studied chemistry at the University of Kerala and obtained his PhD in 2000. After doing postdoctoral research in AIST (2000–2002) and Nanotechnology Research Institute (2002-2003; JSPS Fellow) in Japan, he moved in Pacific Northwest National Laboratory in USA as a Postdoctoral Fellow (2003–2004). Currently, he is a Chief Scientist in Health Research Institute, AIST. In parallel, he is appointed as a PRESTO Researcher of the Japan Science and Technology Agency (JST; since October 2010), a Visiting Professor at the University of Kerala (since 2007), an Adjunct Professor at Southern University (since 2012), and a Guest Professor at the University of Tokushima (since 2012). His current research includes the development of biofunctional and photofunctional nanomaterials, single-molecule spectroscopy and microscopy, optical and magnetic properties of functional nanomaterials, and bioimaging and phototherapy. He is serving as the Associate Editor of the *J. Photochem. Photobiol. C*, Editor of *Nano Reviews*, Editorial Board Member of the *J. Bioengg. Biomed. Sci.*, and Chairman of Asian Nanoscience and Nanotechnology Association (ANNA). He has received many academic recognitions, which include the 14th Gen-nai Award by the Ozaki Foundation, Most Cited Certificate from Analytical and Bioanalytical Chemistry, Distinguished Lectureship Award by the Chemical Society of Japan (2010), Asian and Oceanian Photochemistry Award for Young Scientist (2010), Young Lectureship by the Chemical Society of Japan (2011), and the Japanese Photochemistry Association Award for Young Scientist (2011). Since 2011, he is the Fellow of the Royal Society of Chemistry (FRSC).

1. Introduction

Phototherapy is a form of medical treatment in which light is used to treat diseases such as cancers and peripheral infections to normalize the body and relieve the depression. Photothermal therapy (PTT) and photodynamic therapy (PDT) are the two kinds of phototherapy used for the treatment of diseases so far. In PTT, a photothermal (PT) agent is employed for the selective local heating for healing abnormal cells or tissues; whereas, in PDT, the treatment occurs through a series of photochemical reactions triggered by photoactivated molecules or materials called photosensitizer (PS) drugs. In recent past, nanomaterials are used in different aspects of cancer management in terms of nanomedicine. On the basis of the growing applications of nanomaterials in PDT and PPT of cancer, in this review, we mainly focus on the different formulations of nanomaterials suitable for PTT and PDT.

1.1. Photothermal therapy

Thermal treatment of cancerous cells by applying the local heating to 70 °C and general hyperthermia (heating to 41–47 °C) is known since 18th century [1]. During the local heating or hyperthermia, cells undergo irreversible damage due to the denaturation of proteins and the disruption of the cell membrane. But these thermal treatments damage the healthy tissues as well. More recently, incorporation of laser radiation treatment in thermal cancer therapy opened up a PT method for the selective treatment of cancers. As a result, laser radiation with fiber-optic waveguides finds growing applications in cancer therapy, which is called laser hyperthermia [2]. The main drawback of the laser treatment is the requirement of high-power lasers for the effective stimulation of the tumor cell death [3]. Meanwhile PTT was proposed, in which a PT agent helps the selective heating at the local environment [4]. Basic requirements of PTT are a biocompatible PT agent with large absorption coefficient in the NIR regions and an NIR light source. Thus, surface-modified nanomaterials of carbon, metals, and semiconductors with NIR absorption can be ideal PT agents. The percentage increase in the temperature during PTT strongly depends on the NIR absorption wavelength and the coefficient as well as the power of the excitation light [5]. Illumination of nanomaterials with NIR laser results in an increase in the temperature of the medium, which reaches a maximum value when the NIR absorption maximum coincides with the laser wavelength (Fig. 1).

1.2. Photodynamic therapy

The basic principle underlying PDT of cancers is a chain of photochemical reactions triggered by a photoactivated PS drug. During the irradiation of a PS drug at a suitable wavelength, it will be activated to the excited singlet (S_1) and subsequently to the triplet (T_1) state *via* intersystem crossing. The lifetime of the T_1 state is longer than that of S_1, which facilitates the extended interactions of the PS drug in the T_1 states with the surrounding molecules [6]. Two types of mechanisms, Type I and Type II, are known for

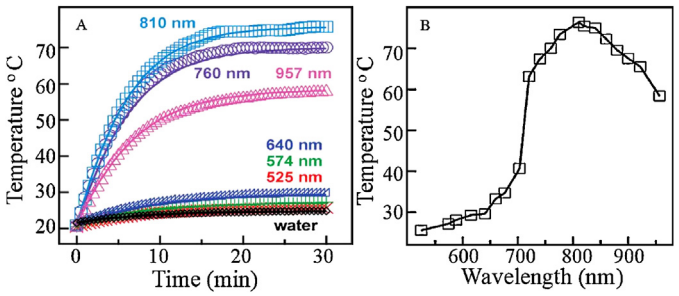

Fig. 1. (A) Experimental (symbols) and calculated (solid line) temperature traces of Au nanorods with different longitudinal plasmon bands, and (B) dependence of the end temperature on the NIR longitudinal plasmon wavelength of the nanorods. Adapted with permission from [5]; Wiley-VCH Verlag GmbH & Co. KGaA.

such interactions at the T_1 state [7]. Type I mechanism involves either the abstraction of a hydrogen atom, or the transfer of an electron between the excited PS and the substrate, which can be a solvent/biomolecule or another PS resulting in the formation of free radicals. Type II mechanism involves the energy transfer between a photoactivated PS and molecular oxygen in the ground state, also called triplet oxygen ($^3O_2$). This energy transfer will result in the formation of a chain of reactive oxygen intermediates (ROI) such as singlet oxygen ($^1O_2$), superoxide, hydrogen peroxide, and hydroxyl radical. Such photophysical and photochemical processes involved in PDT are shown in Fig. 2. The ROI, due to their short lifetime, immediately react with vital biomolecules, causing the selective damage of tumor cells [8]. The destruction of biomolecules is limited to the size of the diffusion sphere of ROI, which is less than 0.1 μm in the case of $^1O_2$ [9]. Hence the localization of PS is crucial for the targeted as well as efficient PDT [10].

2. Nanomaterials in photothermal therapy

Noble metal nanostructures are promising candidates in various aspects of chemistry, physics and biology owing to their unique properties such as large optical field enhancements due to the strong scattering and absorption of light. The optical and PT enhancements of metallic NPs arise from the unique interaction of nanoparticles (NPs) with light. When illuminated, the valance electrons of the metal NPs undergo a collective coherent oscillation with respect to the lattice [11–15]. According to Mie Theory [16], this oscillation is resonant at a particular frequency of electromagnetic field of light, and this phenomenon is known as localized surface plasmon resonance (LSPR). This resonance lies in the visible to NIR region for gold and silver NPs. The LSPR wavelength of metal NPs strongly depends on the size, shape, inter-particle distance, the type of the metal, and the local dielectric constant [12,13,17,18]. For example, gold and silver nanospheres in the 10 nm regime have strong absorption *ca* 520 nm and *ca* 390 nm in water [13]. But with increase in the dimension of the nanoshperes, the LSPR will show a red-shift due to the electromagnetic delay in larger particles. Also, the position of the plasmon band varies from spherical to non-spherical nanomaterials (rod, prism, triangle, tetrapod, cube, shell, *etc.*). In the case of elongated particles, two surface plasmon bands are involved, one along the longitudinal direction and the other along the transverse direction [19–21]. El-Sayed and co-workers have shown that the position of the longitudinal surface plasmon band varies with the aspect ratio (length-to-width ratio) of gold nanorods (GNRs) [16]. When the aspect ratio of the GNR increases, the longitudinal LSPR band red-shifts from the visible to the NIR region (Fig. 3) with progressive increase in the oscillator strength [20,21].

Another way to tune the LSPR is by using a metal nanoshell on the surface of silica NPs [18]. LSPR of gold shell on silica core red-shifts from the visible to NIR region with decrease in the shell thickness due to the enhanced coupling between the inner and outer surface plasmons of the shells [22,23]. The strong enhancement in the absorption of metal NPs results in the localized PT effect under laser illumination, which finds applications in cancer phototherapy. Microscopic images of different plasmonic NPs with tunable LSPR are given in Fig. 4. These include GNRs [24], Au mesoflowers [25], Ag nanocubes [26,27], Ag nanowires [28], Au nanooctahedra [29], Au–Ag nanoboxes [30], Ag/Au nanotubes [28], Au nanocages [30], Au nanoframes [31], and Au nanostars [32]. Despite this large variations in the morphology, nanomaterials used for PTT (Fig. 4) include

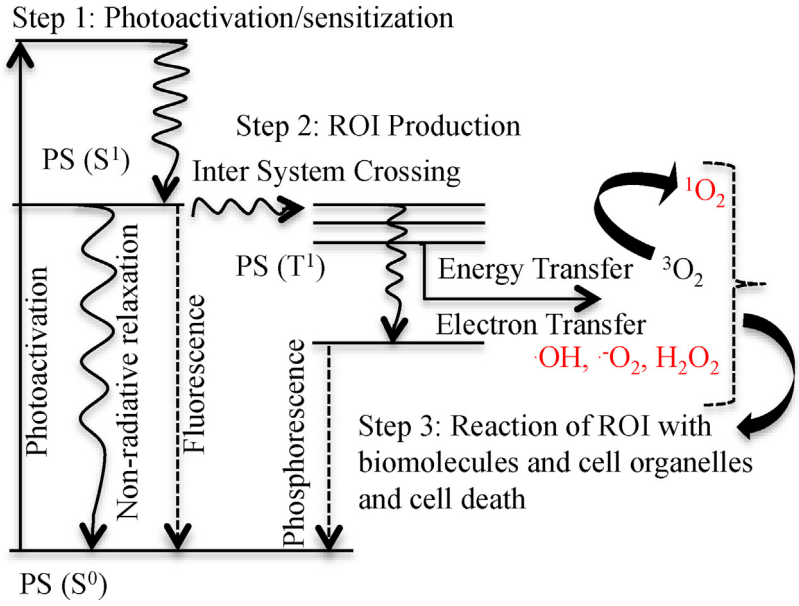

Fig. 2. Photophysical and photochemical processes involved in PDT.

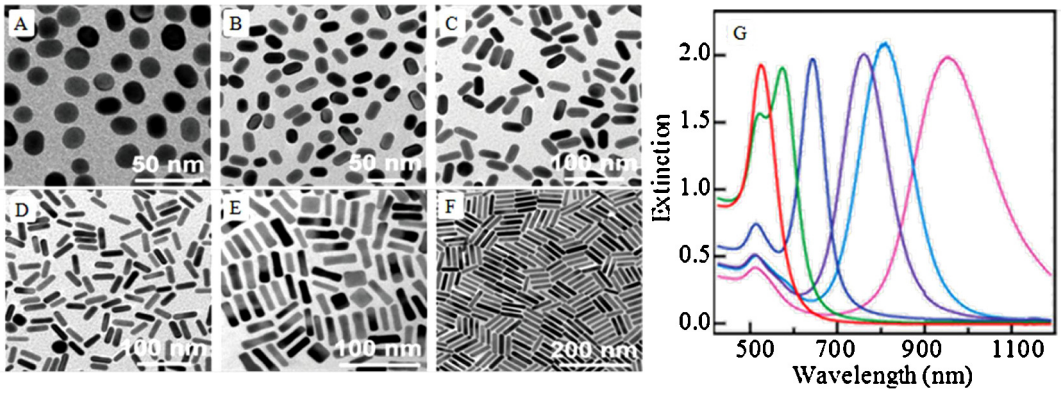

Fig. 3. (A–F) Time-dependent TEM images and (G) UV–vis absorption spectra of GNRs with different aspect ratios.
Adapted with permission from [5]; Wiley-VCH Verlag GmbH & Co. KGaA.

GNRs, GNPs, core–shell NPs [33], gold nanoshells (GNS), multiple twinned NPs, gold nanocubes, gold nanocages, silver triangles [34], carbon nanotubes [35] (CNT), and graphene oxide (GO) [36].

2.1. Gold nanorods (GNRs)

Among the plasmonic nanostructures, GNRs are widely used for both imaging and PTT of cancer cells and tissues due their strong absorption and scattering in the NIR region (650–900 nm). GNRs are elongated NPs with one transverse and one tunable longitudinal surface plasmon bands. GNRs are synthesized by the seed mediated method [37,38] in the presence of cetyltrimethylammonium bromide (CTAB). In this method, small single crystal gold seeds prepared by the sodium borohydride reduction of chloroauric acid in the presence of CTAB are aliquoted into an Au(1) growth solution prepared by the mild reduction of chloroauric acid using ascorbic acid in the presence of $AgNO_3$ and CTAB. By changing the seed to gold salt ratio or the relative concentrations of the added impurities such as silver ions, one can control the aspect ratio of the GNRs. In GNRs, the cationic surfactant (CTAB) forms a bilayer with charged head groups facing outwards [39]. The clinical applications of the as-prepared GNRs are limited due to the cytotoxicity caused by CTAB. To reduce the cytotoxicity caused by CTAB, surface of the GNRs are modified by the coating of a variety of less toxic molecules such as phosphatidylcholine [40], poly(4-styrenesulfonic acid) [41], polyethylene glycol (PEG) [42,43], thiolated polyamidoamine (PAMAM) dendrimers [44] or transferrin [45]. GNRs are also coated using functional nanocarriers such as Pluronic F 68 [46], polylactic acid (PLA) [47], chitosan [48] or poly(acrylic acid) (PAA) [49] in order to reduce the toxicity due to CTAB. Here a suspension of GNRs and the functional nanocarrier is incubated at 4 °C for 12 h. For targeted delivery and PTT, the surface of the GNRs are then conjugated with different biomolecules such as anti-epidermal growth factor receptor (anti-EGFR) antibodies [16], aptamers which are single stranded oligonucleotides that can specifically bind to targeted proteins or peptides [50], arginine–glycine–aspartic acid (RGD) peptides [44], metalloprotease matrix [51], or Herceptin [52].

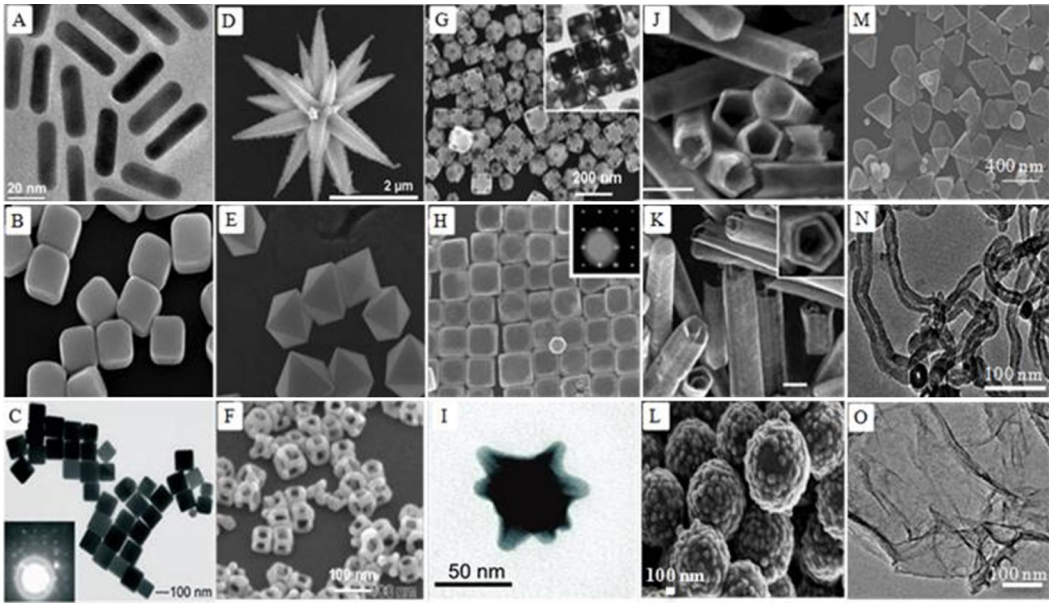

Fig. 4. Various plasmonic nanostructures with absorption in the NIR region. (A) Au nanorods, (B and C) Ag nanocubes, (D) Au mesoflowers, (E) Au nanooctahedra, (F) Au nanoframes, (G) Au nanocages, (H) Au–Ag nanoboxes, (I) Au nanostars, (J, K) Ag/Au nanotubes, (L) silica–Au core–shell NPs, (M) Ag nanotriangles, (N) single walled carbon nanotube (SWCNT), and (O) graphene oxide.
Adapted with permissions from the American Chemical Society [24,29,30,32,35,36]; Springer [25,31]; Science [27]; Wiley-VCH Verlag GmbH & Co. KGaA [26,28,34]; and Elsevier [33].

El-Sayed and co-workers have demonstrated the use of GNRs to be novel contrast agents for both molecular imaging and *in vitro* PTT of cancer cells [16]. Here, anti-EGFR monoclonal antibody-conjugated GNRs are incubated with nonmalignant epithelial cells (Ha Cat) or malignant oral epithelial cells (HOC 313 clone 8 and HSC 3). The anti-EGFR antibody-conjugated GNRs are specifically and effectively bind to the surface of the malignant cells due their overexpression of EGFR. The strong red-scattering from the GNRs bound on the cell membrane is helpful for the discrimination of the malignant cells from the normal cells under dark field imaging (Fig. 5). Recently, Herceptin-conjugated Fe_3O_4-PEG-GNRs are used for targeting, dual-imaging, and PTT of human breast cancer cells (SK-BR-3 cells) [52]. Irradiation of Fe_3O_4-PEG-GNRs with 785 nm NIR laser shows an average increase in the temperature by *ca* 20 and 25 °C for 0.2 and 1.2 nM Fe_3O_4, respectively. The Herceptin present in the Fe_3O_4-GNRs are bound to the HER-2 receptors on the cell membrane, which results in the clustering of the receptors and internalization of a large number of NPs. Irradiation of these cells with 785 nm NIR laser results in the irreversible damage of cells.

El-Sayed and co-workers have demonstrated *in vivo* plasmonic PTT (PPTT) treatment in deep tissue malignancies using GNRs and a portable NIR laser [53]. In this treatment, PEG-GNRs are intravenously injected into the mice and subsequent PPTT shows an inhibition of the average tumor growth over a period of 13 days without having substantial damages to the surrounding tissues. Tae and co-workers have demonstrated PTT *in vivo* using the GNRs loaded Pluronic F 68 nanocarreirs [46]. Here, the GNRs loaded Pluronic F 68 nanocarreirs are injected into nude mice bearing bilateral SCC7 tumors. Irradiation of the tumors with 808 nm laser for 4 min 24 h after injection show significant suppression of the tumor growth with relatively low concentration of GNRs (50 $\mu g\,mL^{-1}$) and low laser fluency (41.5 $W\,cm^{-2}$) compared to the conditions in earlier reports. Yue and co-workers have demonstrated PTT *in vivo* with contrast-enhanced ultrasound imaging using GNR loaded polymeric microcapsules (GNRMCs) composed of PLA [47]. In this case, *in vivo* acoustic enhancement of PTT is demonstrated in the kidneys of New Zealand white rabbits intravenously injected with GNRMCs. An ultrasound image obtained a few seconds after the injection shows an excellent enhancement in the signal from the rabbit kidney, which confirms the ability of the GNRMCs to achieve systemic contrast enhancement of transverse pulmonary capillaries. Bhatia and co-workers have used Raman markers (IR-792, DTTC-765 and DTDC-655) encoded GNRs for *in vivo* PTT and surface enhanced Raman scattering (SERS) imaging [54]. To demonstrate the concomitant PT effects and SERS imaging, three different kinds of SERS-coded GNRs are separately injected at different places in athymic mice implanted with bilateral human MDA-MB-435 tumor cells. Irradiation of the tumors using 810 nm diode laser (2 $W\,cm^{-2}$) results in the rapid heating beyond 75 °C, while the temperature in control mice injected with saline remained under 40 °C. These PT effects are imaged using the infrared thermograpic mapping techniques (Fig. 6).

The random orientation of GNRs in cells results in the minimal absorption of light under linearly polarized excitation. Thus, the efficiency of light absorption and PT using GNRs can be improved by using circularly polarized laser beams. The effects of circularly polarized light on PPTT treatment of cancer cells are demonstrated using the transferrin-conjugated GNRs [45]. The number of scans required for imaging of the cells incubated with transferrin-conjugated GNRs is found to be less for circularly polarized laser beam. Here the PTT using the circularly polarized femtosecond light lowers the threshold of the damage energy by an order of magnitude below the medical laser safety standards. Plasmonic nanostructures; especially, GNRs require relatively high-power laser irradiation in the 1×10^5–1×10^{10} $W\,m^{-2}$ range for PPTT [32]. The high-power laser irradiation causes severe damage to the surrounding healthy cells as well. But recent studies [50] using aptamer-conjugated Au-Ag bimetallic NRs show that the stronger absorption characteristics of these materials can reduce the laser power required for PPTT (8.5×10^4 $W\,m^{-2}$). Here, cancer cells are incubated with aptamer-conjugated GNRs and the cell-death is determined using propidium iodide (PI), a non-fluorescent dye impermeable to live cells, which on the other hand are delivered in dead cells and becomes fluorescent (red) due to intercalation with DNA. The lager absorption coefficient of Au-Ag NRs in the NIR region compared to that of GNRs causes *ca* 93% decrease in the cell viability.

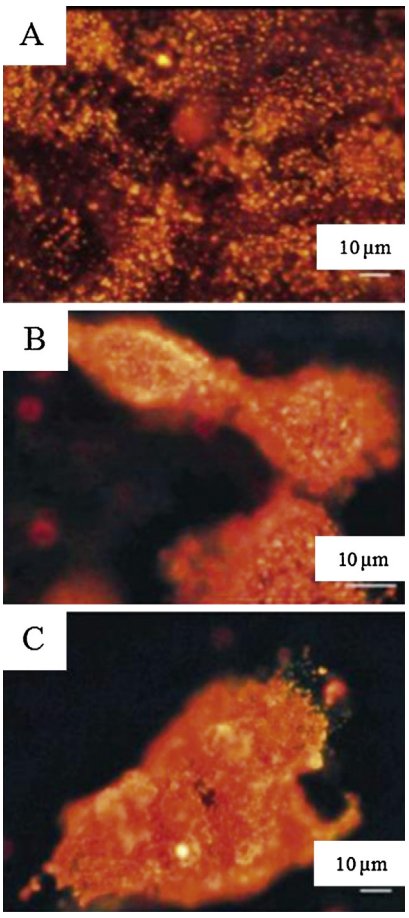

Fig. 5. Light scattering images of cells treated with anti-EGFR/GNRs for 30 min at room temperature (A) HaCaT nonmalignant cells, (B) HSC malignant cells, and (C) HOC malignant cells.
Adapted with permission from [16]; the American Chemical Society.

2.2. Multiple-twinned gold nanoparticles (MTGNPs)

MTGNPs are gold NPs with multiple arms, which enhance the absorption cross-section in the NIR window. The different kinds of MTGNPs used for PTT include branched GNPs [55], gold nanocrosses [56], and popcorn-shaped GNPs (PSGNPs) [57,58]. Branched GNPs are synthesized [59] by the electrochemical reduction of gold ions in presence of sodium citrate [60], followed by replacing the citrate capping with maleimide-PEO-disulfide [61]. Gold nanocrosses with multiple arms are synthesized by the breakage of face-centered-cubic lattice symmetry of gold through the copper-induced twinning [56], whereas, PSGNPs are synthesized by the two-step seed-mediated reduction method [62,63] similar to that used during the preparation of GNRs [37,38]. The biomolecules used for the surface modifications as well as the targeted delivery of

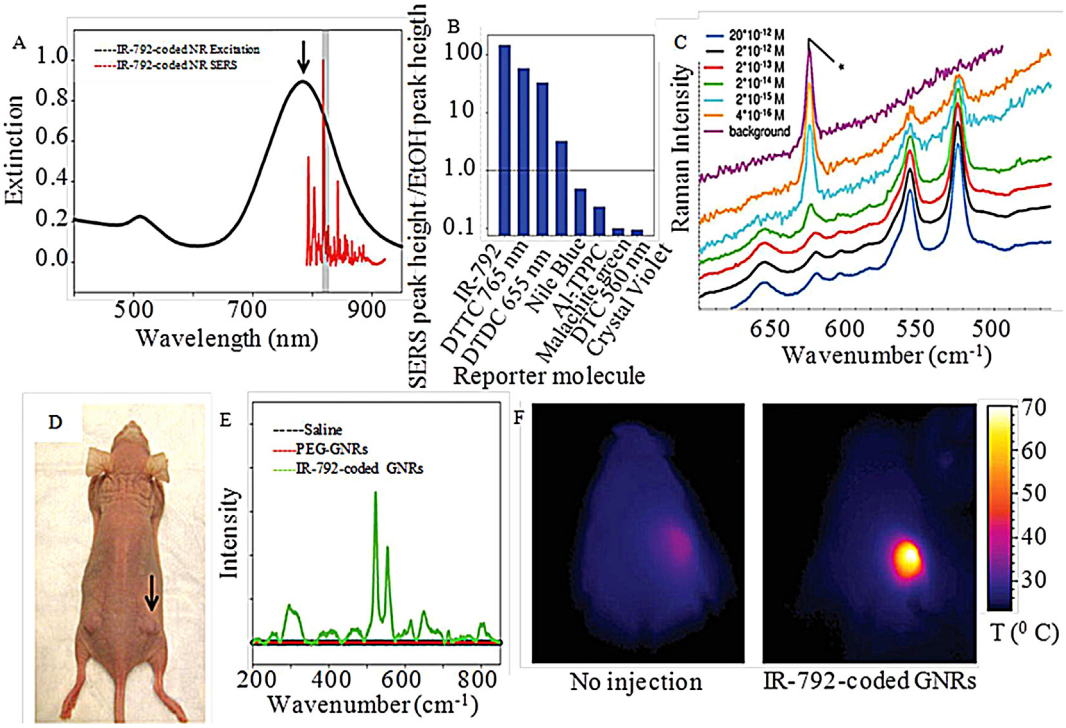

Fig. 6. (A) Overlay of NIR absorption and emission of SERS-coded GNRs. (B) Peak height ratios of the most intense SERS peak of each molecule with respect to the internal ethanol standard at 879 cm^{-1}. (C) SERS spectra of homogenous solutions of IR-792-coded NRs at various concentrations to explore the detection limit. (D) Athymic (nu/nu) mice bearing bilateral human MDA-MB-435 tumors injected intratumorally with SERS-coded GNRs, PEG-GNRs, or saline (arrow) to evaluate the potential for *in vivo* detection and photothermal heating. (E) *In vivo* Raman spectra of IR-792-coded GNRs, PEG-GNRs and saline solution; 10 acquisitions of 4 s are acquired for each spectrum. (F) Infrared thermographic maps of mouse surface temperature 3 min after the onset of irradiation with diode laser (810 nm, 2 W cm^{-12}).
Adapted with persmission from [54]; Wiley-VCH Verlag GmbH & Co. KGaA.

MTGNPs include anti-HER2 nanobodies [50], which are the smallest fully functional antigen binding fragments, monoclonal M3038 antibody [57], and aptamers [58,63,64]. Börghs and co-workers have shown PTT using anti-HER2 nanobodies conjugated branched GNPs in human ovarian epithelial carcinoma cells (SKOV3) using 690 nm laser (38 W cm^{-2}, 5 min) [55]. Here, the cell viability calculated by live/dead cell staining using Calcein AM, a non-fluorescent live-cell stain that becomes green fluorescent when hydrolyzed by intracellular esterases, and PI shows effective PT ablation in the presence of higher concentrations of branched GNPs. Han and co-workers have demonstrated gold nanocross-induced PTT in A549 cells using 900 nm lasers at different intensities [56]. The progress of the PT ablation process detected by following the two-photon emission from the nanocrosses shows a substantial changes in the shape and shrinkages in the size of the cells under 4.2 W cm^{-2} laser intensity and over a period of 30 s. The antibody-conjugated PSGNPs are also used for the selective degradation of MDR B *Salmonella typhimurium DT104* [57], a multiple drug resistant food poison. The localized heating during the NIR irradiation (670 nm) of contaminated food causes the rapid degradation of MDR B [62]. More recently the SERS and PTT properties of multifunctional PSGNPs are exploited during the diagnosis and treatment of prostate cancer [58]. Here, the diagnostic tool is the significant enhancement in the Raman signal of Rhodamine B (Rh6G) that is conjugated to PSGNP through aptamers. Irradiation of prostate cancer cells incubated with Rh6G functionalized PSGNPs results in the permanent damage of the cells due to the localized heating offered by the plasmonic PSGNPs, which is higher than the PT response by GNRs. Also, the aptamer-conjugated hybrid nanomaterials composed of PSGNPs and SWCNT are used for the diagnosis and selective PTT of cancer cells [64]. Here, PSGNPs are attached to the surface of SWCNT through the para-aminothiophenol moiety. Here, the hybrid nanomaterials provide significant enhancement in the Raman signal intensity for D and G bands of SWCNT by 3 orders of magnitude. By the combined PT effects offered by PSGNP and SWCNT, local heating up to 60 °C and efficient killing of cancer cells are achieved under 785 nm laser (1.5 W cm^{-2}) excitation, which is more significant than that offered by SWCNT alone. The visualization of the PT effect of PSGNP by the NP surface-energy transfer (SET) approach using dye-labeled RNA is reported recently [62]. Here, the aptamer functionalized PSGNPs are hybridized with Cy3-modified RNA (CTG GTC ATG GCG GGC ATT TAA TTC), which is complementary to the aptamer extension sequence. Subsequent excitation of Cy3 molecules results in the energy transfer from Cy3 to the NP surface, which is efficient due to the close-proximity between the dye and the NP.

2.3. Nanocubes, nanocages and nanotriangles

Recently, gold nanocubes, gold nanocages and silver nanotriangles are used for PTT. The gold nanocages with absorption maximum *ca* 800 nm are synthesized by the galvanic replacement reaction between $HAuCl_4$ and silver nanocubes [65]. Luminescent gold nanocubes [66] are synthesized by the seed-mediated method similar to the one developed for GNRs by El-Sayed and Murphy [37,38]. Chitosan-Ag triangles [67] (Chit-AgNTs) are also prepared by the seed-medicated method [68]. Here, the silver seed particles prepared by the reduction of silver nitrate using sodium borohydride in presence of trisodium citrate are aliquoted into a silver growth solution prepared by the mild reduction of silver nitrate using ascorbic acid in presence of chitosan. Xia and co-workers [65] have demonstrated the PT effect of anti-HER2 conjugated gold nanocages in breast cancer cells (Sk-BR-3). During the PTT, the cells targeted with immuno gold nanocages responded to the laser

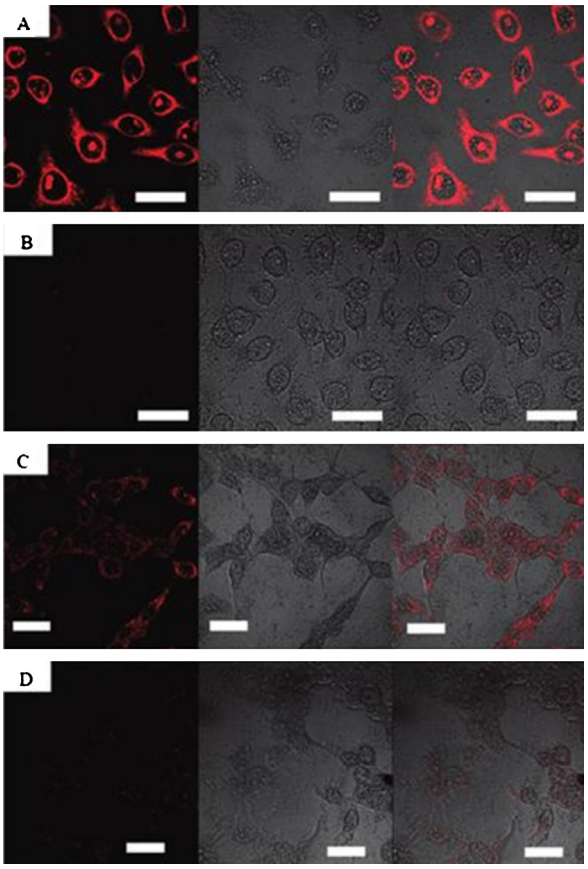

Fig. 7. Detection of cell damage using PI in nanocube loaded cells. Here, the fluorescence of PI is detected in the 580–640 nm channel. (A) Nanocube-loaded human liver cancer cells (QGY) irradiated with 532 nm laser for 15 min (4 W cm^{-2}). (B) Nanocube-loaded QGY cells without irradiation. (C) Nanocube-loaded human embryonic kidney cells (293T) irradiated with 532 nm laser for 15 min (4 W cm^{-2}). (D) Nanocube-loaded 293T cells without irradiation. Left, PI fluorescence images; middle, DIC images; and right, merged images. Scale bars are 30 μm. Excitation light source for fluorescence imaging is 488 nm laser.

Adapted with permission from [66]; the American Chemical Society.

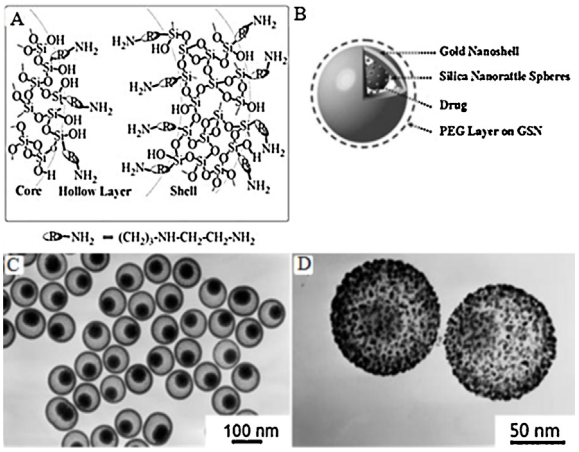

Fig. 8. (A) Structures of silica nanorattle (SN), (B) drug-loaded PEGylated-gold-shelled SN, and (C–D) TEM images of SNs and gold seeds attached to SNs.

Adapted with permission from [79]; Wiley-VCH Verlag GmbH & Co. KGaA.

irradiation immediately, which is helpful for controlling the cell death by adjusting the laser power and irradiation time. PT ablation studies of luminescent gold nanocubes [66] in human liver cancer cells (QGY), and human embryonic kidney cells (293T) using 532 nm cw laser (4 W cm^{-2}) show the complete cell death, which is evaluated by the PI staining of the dead cells (Fig. 7). The PT effect of gold nanocubes is essentially similar to that of GNRs [66]. PTT using Chit-AgNTs shows efficient cell death compared to that by GNRs [68], which is attributed to the highest thermal conductivity of silver (429 W m^{-1} k^{-1}) and the triangular flat structure of the NPs.

2.4. Gold nanoparticles (GNPs)

GNPs find their place in PTT since 2003 [69,70]. Pitsillides and co-workers have first demonstrated the selective damage of cells using 20–30 nm diameter GNPs illuminated with 532 nm laser [71]. Soon after, El-Sayed and co-workers have demonstrated the PPTT of cancer cells using anti-EGFR antibody conjugated GNPs [1,11,53,72]. Subsequently, by targeting transferrin-conjugated GNPs to breast cancer cells, the laser power required for PTT was reduced by two orders of magnitude [72]. GNPs stabilized with pH sensitive ligands are also used for PT ablation [73]. During the pH change, the GNPs stabilized with pH sensitive ligands aggregate, which in turn shifts the absorption band from the near-red to the far-red region. This shift in the absorption band to longer wavelength is useful for PTT as it enables the effective excitation of the PT agent *in vivo*. PTT combined with drug release using NPs was demonstrated later using poly(lactic-co-glycolic acid)-gold half-shell NPs (PLGA) [74]. The drug doxorubicin is encapsulated within the biocompatible and biodegradable PLGA NPs and finally a gold layer was deposited on the surface of these NPs. During the NIR irradiation, doxorubicin loaded in the PLGA is released rapidly due to the degradation of PLGA. The PT treatment combined with the drug delivery improves the therapeutic efficiency and shortens the treatment time. Similarly, GNPs shelled with biocompatible PEGylated nanogel are used for PTT [75], and indocyanine green (ICG)-labeled GNPs are used for the combined PTT and PDT of cancer cells [76]. Here, the effective interaction of the free electrons of metal NPs with the photoactivated state of the fluorophores induces a dipole nature to the system, which provides a relatively high photostability to the dye molecules even at higher temperatures. Hence the combined PPT and PDT using the dye-labeled GNPs is an efficient method for the treatment of cancer.

2.5. Core–shell nanoparticles

Among a wide variety of plasmonic nanomaterials, gold-silica nanoshells gained much attention in PTT due to their strong absorption or scattering in the NIR region [77]. Different core-shell NPs used in PTT include gold shelled-silica NPs (GSNPs) [18], gold-speckled silica NPs (GSSNPs) [78], gold-shelled silica nanorattle (GSN) [79], gold-nanoshells with carboxylated polystyrene spheres (GNSCPSs) [80], gold-nanoshelled microcapsules (GNSMCs) [81], gold-shelled Fe_3O_4 NPs [82], and gold-shelled upconversion NPs-Fe_3O_4 complex (GS-UCNPs-Fe_3O_4) [83,84]. Core-shell NPs in this contest are spherical particles consisting of dielectric silica cores and metallic shells having nanometer thickness. Here, the surface of monodisperse silica core synthesized by the Stöber process [85] is functionalized with organosilane molecules such as 3-aminopropyltriethoxysilane (APTES). Small gold NPs with 1–2 nm diameter are then covalently attached on the surface of the organosilane functionalized silica core *via* the amine group [18]. The surface of gold-silica NPs is modified mainly using PEG [86] or methoxy-PEG-thiol [79], which improves their biocompatibility and water solubility. GSSNPs composed of silica core with irregular gold nanodomains are synthesized by a microemulsion method [78], which involves tetraethyl orthosilicate (TEOS) and aminopropyl triethoxysilane (APTS). Gold domains are deposited

on the surface of the silica matrix *via* free amine functional sites. SN core is fabricated by the core-etching of the organic-inorganic hybrid solid silica spheres (HSSs) using hydrofluoric acid [87], and gold-nanoshell are then grown on the surface of the SNs by the seed-mediated method (Fig. 8) similar to the one used for the synthesis of GNSCPs [76]. GNSMCs are synthesized [81] by the electrostatic adsorption of citrate-stabilized gold NPs on the surface of polymeric microcapsules prepared by the emulsifier-free emulsion polymerization using potassium persulfate as the anionic initiator [87]. Gold-shelled Fe_3O_4 NPs are synthesized starting from the thiol functionalized Fe_3O_4-silica nanospheres [88]. Here, the thiol functionalized Fe_3O_4-silica nanospheres are formed through the self-assembly of the amphiphilic block copolymers polystyrene-b-poly(acrylicacid) and Fe_3O_4 NPs followed by the cross-linking with 3-mercaptopropyltrimethoxysiliane (3MPS). Finally, gold nanoshells are decorated on the surface of the silica spheres by the seed-mediated reduction method [89]. The GS-UCNPs-Fe_3O_4 is prepared by the electrostatic interaction of Fe_3O_4 NPs with $NaYF_4$-based UCNPs [83,84,90,91] followed by the seed-mediated fabrication of gold shell [83,93]. The conjugation of GS-UCNPs-Fe_3O_4 with PEG and folic acid (FA) improves their biocompatibility and targeted delivery [83,84,90,91]. UCNPs referred here are the nanocomposites of transition metal ions, lanthanide ions or actinide ions doped into the solid-state host, which emits higher energy light under lower energy excitation [92,94]. A variety of core materials and dopants are used for the synthesis of UCNPs, among which the micrometer-sized Er^{3+}/Yb^{3+} or Tm^{3+}/Yb^{3+} co-doped hexagonal $NaYF_4$ shows the highest upconversion efficiencies [95].

West and co-workers have first demonstrated PTT using the gold nanoshells nearly a decade ago [69]. Subsequently, Drezek and co-workers have shown the nanoshell-based PTT of human breast carcinoma cells [69]. West and co-workers have later accomplished PTT more effectively in solid tumors by the direct injection of PEGylated nanoshells [86]. Here, the temperature fluctuations after the irradiation was mapped using the magnetic resonance thermal imaging (MRTI). Gröbmyer and co-workers have used FITC-loaded GSSNPs for the PTT of A549 lung carcinoma cells under 785 nm excitation [78]. Here, the fluorescence from FITC is used for visualizing the internalization of GSSNPs in A549 cells and trypan blue staining for necrosis. Tang and co-workers have demonstrated PTT *in vivo* in hepatoma 22 (H22) solid tumors using PEG-GSN and NIR laser irradiation (2 W cm^{-2}) [79]. Here, the weight of the tumor drastically decreased during the course of the photothermal ablation. During this treatment, the temperature of the tissue raises due to electron-phonon and phonon-phonon interactions [17] in PEG-GSNs, which is detected by infrared thermal imaging (Fig. 9). Eventually, the drug releasing property of PEG-GSNs is demonstrated for the anticancer drug docetaxel (DOC). Here, the amount of DOC loaded in PEG-GSNs (*ca.* 1.08 μg $μg^{-1}$ PEG-GSNs) is greater than that in SNs (*ca.* 0.48 μg $μg^{-1}$ SNs). Also, the raise in the temperature during the course of the PTT results in the targeted delivery of DOC.

Recently, GS-UCNPs-Fe_3O_4 (MFNP) is used for the combined PTT and multimodal imaging [83,84]. Here, the incubation of HeLa cells with MFNP (0.05 mg mL^{-1}) followed by laser illumination (808 nm laser, 1 W cm^{-2}) results in the destruction of cancer cells. The intrinsic photoluminescence of the UCNPs and the magnetic properties of Fe_3O_4 NPs in MFNP are utilized for mapping the course of hyperthermia. The magnetic properties of PEG-MFNP are also utilized for the magnetically controlled PTT, for which HeLa cells are incubated with PEG-MFNP under an external magnetic field and photoactivated for 5 min. As a result of the combined magnetic field and photoactivation, the cells near to the magnetic field are selectively destroyed. On the other hand, the cells located away from the magnetic field remained essentially unaffected (Fig. 10).

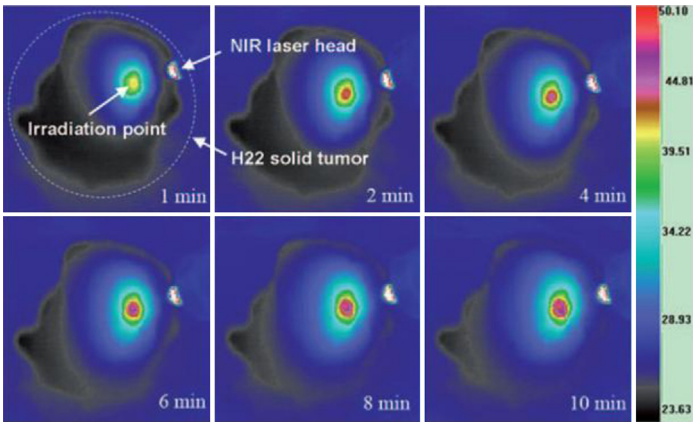

Fig. 9. Infrared thermal images of an excised PEG-GSNs-injected H22 solid tumor sample at different time under NIR laser irradiation. The color bar represents the relative temperature values in °C. The dashed circle indicates the H22 solid tumor. Adapted with permission from [79]; Wiley-VCH Verlag GmbH & Co. KGaA.

In vivo PTT using the PEGylated nanoshells [18] was first demonstrated by West and co-workers. Here, the PEGylated nanoshells are intravenously injected into mice and allowed to circulate for 6 h before illuminating with a diode laser (808 nm, 4 W cm^{-2}, 3 min). Tumors from the mice were disappeared within 10 days of the treatment using the nanoshells [86]. The strong scattering and absorption of the nanoshells in the NIR window are simultaneously utilized for combined PTT and optical coherence tomography [96] (OCT) imaging, which is an optical analogue to ultrasound imaging with relatively good penetration depth (1–2 nm) and resolution (~1–10 μm) [86]. Here, the OCT images collected 20 h of the post injection show an enhanced brightness in the tumor tissues compared to the normal tissues. Subsequently, silica-gold nanoshells are used for demonstrating the PTT of glioma in murine xenograft, which is the most aggressive primary brain tumor [97]. In this case study, the PEGylated silica-gold nanoshells are injected into mice implanted with firefly luciferase labeled U373 human glioma cells. NIR (800 nm) irradiation of the tumor in mice treated with PEGylated silica-gold nanoshells 24 h of post injection shows considerable reduction in the tumor size. Meanwhile, the DOC loaded PEG-GSN has been used for evaluating the *in vivo* PTT and chemotherapy in tumor bearing mice. In this evaluation, PEG-GSN-DOC is intravenously injected into mice at a concentration of 200 μg and irradiated with NIR light (2 W cm^{-2}). The weight of tumor in the mice treated with PEG-GSN-DOC is considerably decreased compared to that in control mice. Here, the release of DOC from the surface of GSN nanoparticle occurs due to the local heating experienced during the hyperthermia. In another case study, GNSCPSs are also utilized for evaluating PTT in Lewis lung carcinoma [80]. Here, a solution of GNCPSs is injected into the mice bearing human Lewis lung carcinoma tumors and irradiated with NIR light (808 nm, 4 W cm^{-2}). Interestingly, tumors in the treated mice are almost disappeared 12 days after the first laser treatment. Recently, GNSMCs are used as an agent for both PTT and ultrasound contrast imaging [81]. The *in vivo* acoustic ultrasound enhancement studies are carried out in New Zealand white rabbits. The ultrasound contrast images collected from the kidney of the rabbits show more enhancements in the pulse-inversed harmonic imaging (PIHI) mode in contrast with the conversional B mode. Similarly, silica-shelled Fe_3O_4 NPs are used for bimodal-imaging and *in vivo* PTT [82]. The *in vivo* T_2 weighted MR images collected from the tumor site after the injection of silica-shelled Fe_3O_4 NPs show an enhanced darkening with *ca* 38% drop in the T_2 signal intensity. Similarly, GS-UCNPs-Fe_3O_4 NPs are used for the combined bimodal-imaging and *in vivo* PTT in mice bearing KB tumor.

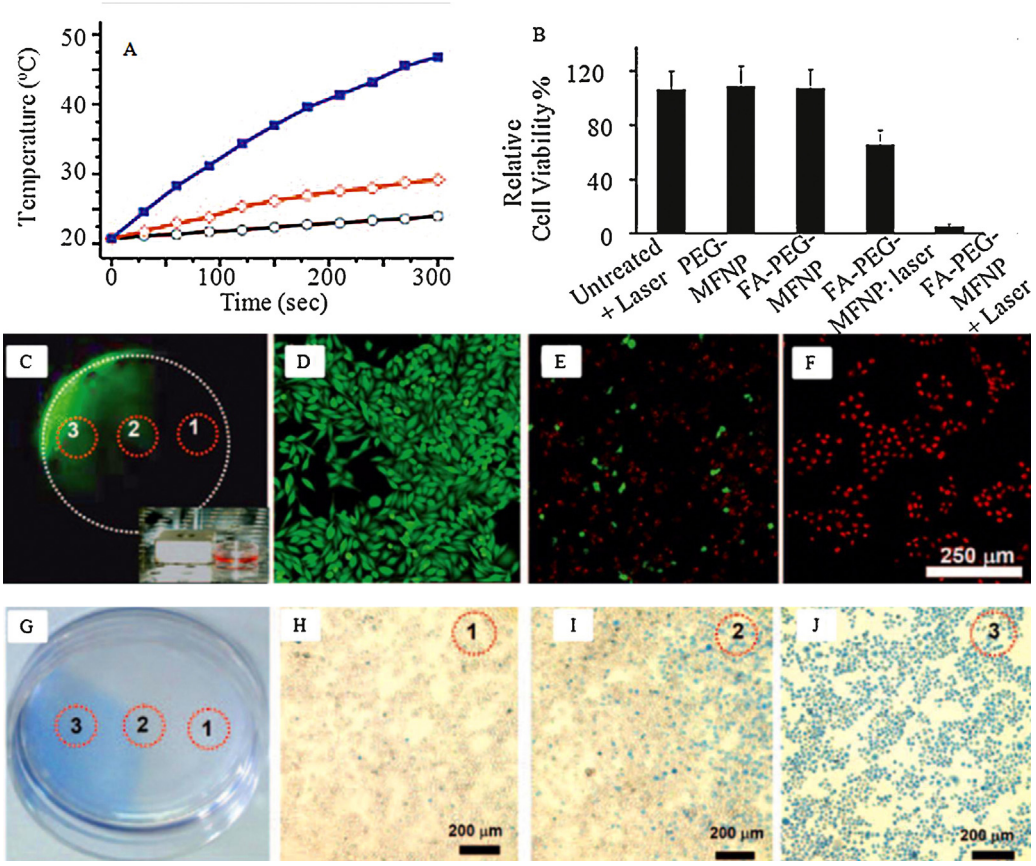

Fig. 10. (A) The heating curves of water and solutions of UCNPs-Fe_3O_4 nanocomposite and MFNP under 808 nm laser irradiation. (B) Relative viabilities of KB cells treated with PEG-MFNP- or FA-PEG-MFNP with or without laser irradiation. (C) Upconversion luminescence image of HeLa cells in a culture dish taken, using the Maestro *in vivo* imaging system (980 nm excitation), after incubation with PEG-MFNP under an applied magnetic field. Inset: photograph showing the experimental setup. A magnet is placed close to the cell culture dish. (D–F) Confocal images of calcein AM (green, live cells) and propidium iodide (red, dead cells) co-stained cells after magnetically targeted PTT. (G) Digital photograph of the cell culture dish after the magnetically targeted PTT and trypan blue staining. (H-J) Optical microscopy images of trypan blue stained cells after the magnetically targeted PTT.

Adapted with permission from [84]; Wiley-VCH Verlag GmbH & Co. KGaA.

Here, the fluorescence images collected from the liver and tumor sites show a strong upconversion emission from the NPs. The T_2-weighted MR images collected after the intravenous injection also show a darkening effect in the liver. Furthermore, the *ex vivo* upconversion luminescence images show a high density of the NPs in the tumor milieu and the reticuloendothelial systems including the liver, spleen, lungs and bone marrow. Finally, the GS-UCNPs-Fe_3O_4 NPs are used for the mapping of lymph nodes in mice. Here, the NPs accumulated in the primary lymph nodes are visualized by the *in vivo* UCL imaging 2 h after the injection (Fig. 11).

2.6. Gold nanoshells (GNS)

GNS are composed of a thin gold wall and a hollow interior with a strong tunable plasmonic absorption in the NIR region. GNS are synthesized by the cobalt NP-mediated reduction of chloroauric acid [98]. At first, cobalt NPs are synthesized by the sodium borohydride reduction of a deoxygenated and deionized aqueous solution of sodium citrate and cobalt chloride under the nitrogen atmosphere. Subsequently, GNS are synthesized by the addition of chloroauric acid to the as prepared cobalt NPs. During this process, cobalt NPs reduces the gold ions to form a gold NP layer, while at the same time, cobalt NPs are oxidized into cobalt oxide.

PEGylation improves the biocompatibility and solubility of the as-synthesized GNS [99,100]. To utilize GNS for both *in vitro* and *in vivo* targeted delivery and PTT, the surface of GNS are conjugated with different biomolecules such as anti-EGFR antibody [101] or NDP-MSH (α-melanocyte-stimulating hormone [Nle^4,D-Phe^7]) [102]. Here, the NDP-MSH is synthesized using the *p*-methoxybenzhydrylamine resin [103]. Li and co-workers have shown the potentials of EGF-conjugated GNS for PPTT [101]. Exposure of an aqueous solution of the conjugate to 8 W cm^{-2} laser results in the elevation of local temperature up to 41.5 °C and an effective destruction of the cells treated with the conjugate. In a subsequent report, they have shown the potentials of GNS-NDP-MSH for the *in vivo* targeting of melanocortin type-1 receptor (MC1R) over-expressed in melanoma [102]. Here, PEG-GNS-NDP-MSH is intravenously injected into nude mice bearing murine B16/F10 melanoma. The intracellular uptake of the NPs and the distribution of h-arrestin are monitored by the [^{18}F] fluorodeoxyglucose positron emission tomography (PET). The PET images collected from the mice treated with PEG-GNS-NDP-MSH show a reduced uptake of [^{18}F] fluorodeoxyglucose in the tumor, which is similar to that observed for mice injected with PEG-GNS or saline [99,100]. Recently, the same group has shown the PT effects of GNS in mice bearing human glioblastoma (U87-TGL), which is monitored by photoacoustic tomography (PAT) [103]. Mice injected with RGD-PEG-GNS are exposed to the NIR laser. The PAT images obtained 24 h after the injection clearly highlights the brain tumor and its location. PAT signal ratio of tumor-to-normal tissues is twice for the mice injected with RGD-PEG-GNS than the controls. Here, the progress of PTT in mice is studied using the time-dependent magnetic resonance temperature imaging.

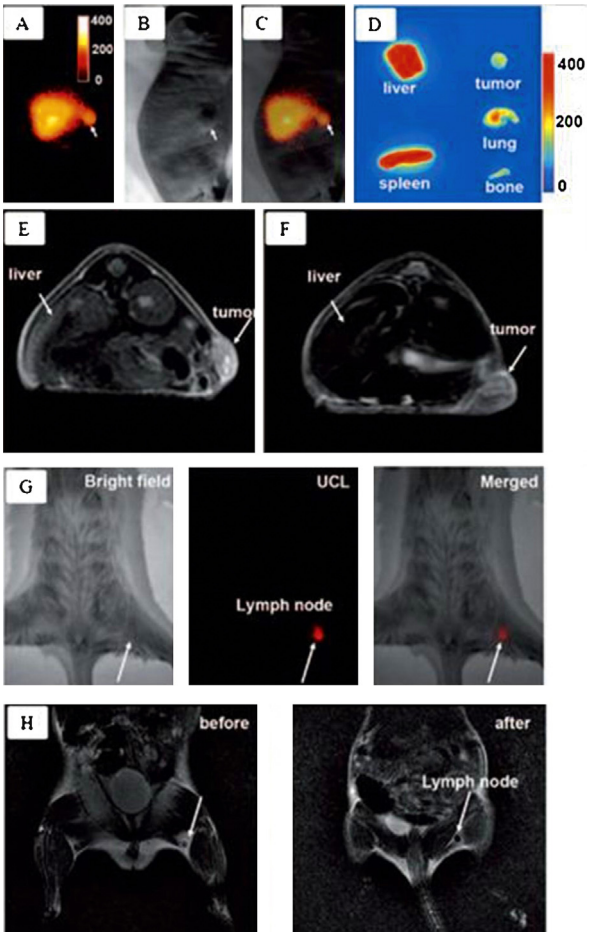

Fig. 11. The upconversion luminescence (UCL) (A), bright field (B), and merged (C) images of a KB tumor-bearing mouse obtained one hour after intravenous injection of PEG-GS-UCNPs-Fe_3O_4 NPs. Strong upconversion luminescence signal is detected from the liver and tumor sites (arrow). (D) *Ex vivo* UCL showing accumulation of the NPs in the liver, spleen, tumor, bone marrow, and lungs of the mouse over a period of 24 h. The UCL signals from other organs are barely detectable. (E and F) T2-weighted images of KB-tumor bearing nude mice with (E) and without (F) injection of the NPs. Obvious dark contrast is detected from the liver and tumor sites. (G and H) Multimodal UCL (G) and MR (H) lymphangiography obtained for a mouse injected with GS-UCNPs-Fe_3O_4 NPs. MR images are taken before (left) and after (right) the injection.

Adapted with permission from [83]; Wiley-VCH Verlag GmbH & Co. KGaA.

2.7. Carbon nanomaterials

The large NIR absorption coefficient ($6.2 \times 10^6\ M^{-1}\ cm^{-1}$) [104,105], mechanical flexibility, large surface area and small diameter of carbon nanotube (CNT) make it a good candidate for PTT. Similarly, graphene and reduced graphene oxide (RGO) have been proposed to be promising candidates for PTT due to their strong optical absorption in the NIR window. PEGylation improves the biocompatibility and water-solubility of both single walled carbon nanotube (SWCNT) and RGO [106,107]. Conjugation of SWCNT [108,109] or RGO [110] with FA or RGD peptide is useful for the targeted intracellular delivery of these carbon nanomaterials.

To-date there is only a limited number of reports on the applications of functionalized CNT or GO for PTT. For example, the *in vitro* PTT of FR-positive mouse mammary tumor cells (EMT6) incubated with the FA-PEG-SWCNT conjugate followed by irradiation with 980 nm laser ($0.5\ W\ cm^{-1}$) results in the considerable decrease of cell viability [106]. Similarly, RGD peptide-functionalized RGO is used for the selective uptake and *in vitro* PT ablation in U87MG cancer cells [106]. Drug delivery and multimodality in PTT are accomplished on GO platforms such as doxorubicin-loaded PEG-GO [111] and PEGylated GO with Fe_3O_4 NPs (GO-Fe_3O_4-PEG). Here, the magnetic field-assisted delivery of doxorubicin using GO-Fe_3O_4-PEG shows enhanced uptake of GO-Fe_3O_4-PEG-DOX in murine breast cancer 41 cells. The cell viability measured using calcein AM/PI double staining shows the selective damage of cells within the external magnetic field. PTT using quantum dots (QDs)-tagged GO in MCF-7 cells under 808 nm laser illumination ($2\ W\ cm^{-2}$) shows an efficient cell-death as well as a slow photothermal degradation of QDs [112].

More recent *in vivo* investigations using bioconjugated carbon nanomaterials show their great potentials for PTT of cancers. For example, NIR (980 nm, $1\ W\ cm^{-2}$) PTT using the mitochondria-targeting PEG-SWCNT conjugate [106] in female Balb/c mice bearing EMT6 tumor shows an increase in the temperature at the tumor site within 5 min of irradiation. Here, the tumor size in the treatment group is drastically reduced with complete disappearance of the tumor and the development of fibrotic tissues 30 days after the treatment. The changes in the surface temperature of the tumor during the PTT using FA-PEG-SWCNT are monitored using IR thermal imaging [108]. Similarly, the PT effect of SWCNT under low-power laser irradiation is studied in C3H/HeN mice model of squamous cell carcinoma (SCCVII) by following the characteristic G-band of SWCNT in the Raman spectrum [112]. SWCNTs functionalized with PEGylated phospholipids [113] and glycated chitosan-FICT [114] conjugate are utilized for *in vivo* PTT in Balb/c mice bearing 4T1 murine breast tumor and EMT6 tumor, respectively. Also, the photoluminescence of SWCNTs was utilized for near-IR tumor imaging [113]. Interestingly, tumor is completely disappeared for the treated mice without inducing any toxic side effect (Fig. 12). Gold-shelled SWCNT with improved NIR absorption coefficient and reduced toxicity are also recently used for PTT [115]. The *in vivo* PTT using PEGylated nanographene sheets (PEG-NGS) [110] in Balb/c mice bearing 4T1 tumor followed by NIR irradiation (800 nm) shows the complete disappearance of the tumor with no further tumor regrowth over a period of 40 days. More recently, combined PTT and PDT is practiced using chlorine e6 (Ce6)-loaded PEG-GO conjugate [116]. Here, Ce6 is loaded on the surface of PEG-GO by the supramolecular π–π stacking. One of the advantages of the PEG-GO conjugate in this case is an improved cellular uptake of Ce6 assembled on the conjugate and thus efficient PDT of cancer cells.

3. Nanomaterials in photodynamic therapy

An ideal PS drug has high absorption coefficient in the 650–850 nm region, high yield of $^1O_2$, solubility under physiological conditions, large tumor selectivity, poor damage of healthy tissues and fewer side effects such as mutagenic, carcinogenic and allergic effects. The main advantages of PDT over radiation therapy and chemotherapy are its site-specific photoactivation of targeted PS drugs with visible or NIR light and minimal damage of the normal tissues. The main two classifications of PS drug are porphyrins and non-porphyrins. Hematoporphyrin (Hp) isolated from hemoglobin is among the first generation PS drug that has several limitations such as prolonged accumulation in tissues and toxicity. Due to these drawbacks of Hp, many second-generation PS drugs having less toxicity, short accumulation in tissues and short NIR absorption are developed. However, the hydrophobicity and poor tumor selectivity of the second-generation PS drugs are limitations for their PDT applications. In the third- generation PS drugs, the targeted delivery using carrier molecules is helpful for reducing their accumulation in healthy tissues. Classical examples of non-porphyrin PS drugs include hypericin, methylene blue, cyanine dyes, and rhodacyanine dyes. Among the several PS drugs, photofrin® (porfimer sodium)

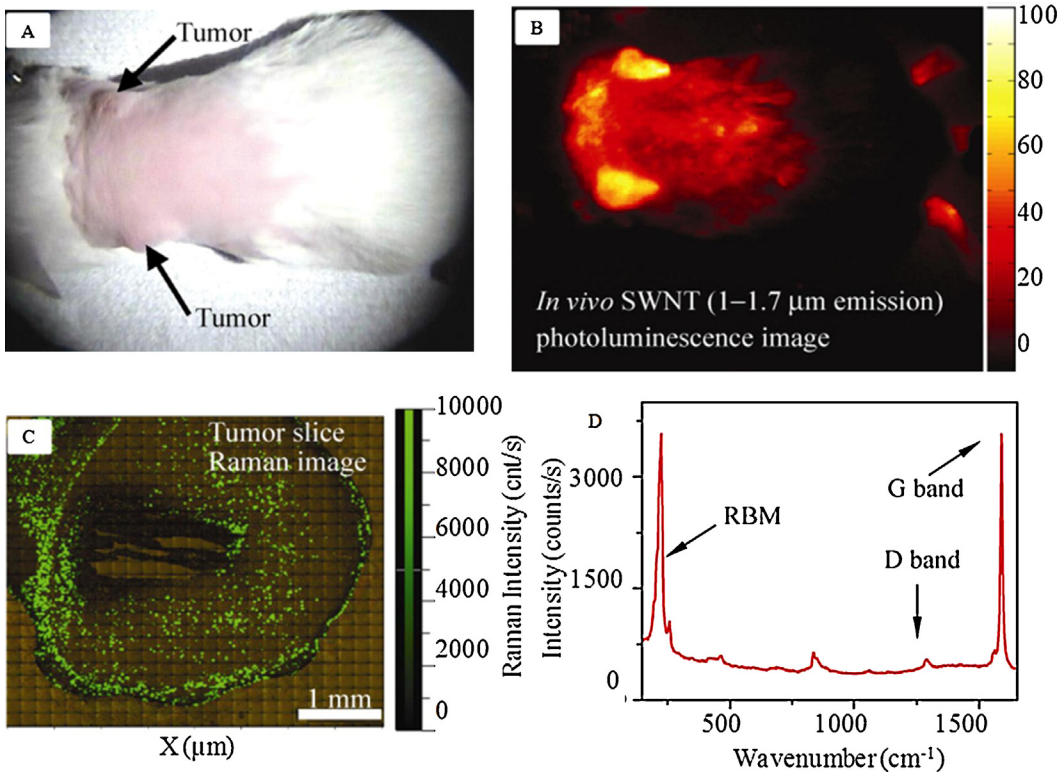

Fig. 12. *In vivo* NIR imaging using photoluminescence from the SWCNT. (A) Optical image of a Balb/c mouse with two 4T1 tumors (indicated by arrows). (B) NIR photoluminescence image taken 48 h post-injection. (C) A Raman image (the green color represents the intensity of the Raman G band) of SWCNTs showing the distribution of SWCNTs in a 10 μm thin slice of tumor. (D) A Raman spectrum of a SWNT solution. The strong characteristic G peak at 1600 cm^{-1} is used for Raman imaging.
Adapted with permission from [113]; the Springer.

having absorption maximum *ca* 625–630 nm is the first PS drug to find clinical application (1993). Even though photofrin® has been used for PDT of different cancers, its poor water solubility is a major limitation. The first approved second-generation PS drug in clinic is 5,10,15,20-tetrakis(m-hydroxyphenyl)chlorin (2002) which has high quantum yield of $^1O_2$ generation. Other second-generation PS drugs clinically accepted for PDT are aminolevulinic acid, porphycenes, and phthalocyanines. Among these drugs the last two are promising due to their strong absorption in the red, long-lived triplet state, and high triplet quantum yields. Despite all these developments, PDT is still not well adapted in clinical practice because of different factors such as toxicity, poor solubility of the PS drug in water, and poor selectivity without affecting the normal tissues. Recently, nanomaterials conjugated with PS drugs find considerable attention in PDT. A combination of nanomaterials and PS drugs forms a class of nanomedicine. Among the wide variety of nanomaterials, quantum dots (QDs), upconversion NPs (UCNPs), silica NPs, plasmonic NPs, carbon nanomaterials, polymer NPs, liposomes and micelles are being combined with PS drugs and applied in PDT both *in vitro* and *in vivo*.

3.1. Quantum dots (QDs)

Quantum dots are NPs in which the electrons and holes are three dimensionally confined within the exciton Bohr radius of the materials. The quantum confinement renders unique optical properties such as narrow emission band and size-dependent tunable photoluminescence [117–119]. Exceptional photostability, large surface to volume ratio, and large two-photon absorption cross-section of QDs make them promising candidates for bioimaging and PDT [8,120–123]. In general, QDs used in PDT of cancer models include CdSe, CdTe, CdSe/ZnS and InP/ZnS. CdSe or CdTe QDs are synthesized by the pyrolysis of organometallic precursors of cadmium and Se or Te [117]. The synthesis of CdSe or CdTe QDs involves a nanocrystal nucleation-growth reaction of dimethyl cadmium ($CdMe_2$, 13.35 mmol) dissolved in trioctylphosphine (TOP, 25 mL) with TOPSe or TOPTe dissolved in TOP (15 mL) at 230–300 °C. Later, the CdSe or CdTe QDs synthesis is modified by replacing the toxic and volatile $CdMe_2$ with safer and greener precursors such as cadmium oxide and cadmium acetate [124].

Burda and co-workers have first demonstrated the use of QDs in PDT by linking a silicon phthalocyanine (Pc4) to QDs through an alkyl group on the axial substituent of Pc4 [125]. Here, the PS drug is indirectly excited by the Förster resonance energy transfer (FRET) from QDs, which enables the production of $^1O_2$ at *ca* 5% quantum yield in toluene. The production of $^1O_2$ is monitored by following its NIR luminescence *ca* 1270 nm. Subsequently, peptide-coated QD-PS conjugates are used for the production of $^1O_2$ at high quantum yields [126]. For example, Weiss and co-workers tethered Rose Bengal (RB) or Ce6 [127] on the surface of CdSe/ZnS QDs and the production of $^1O_2$ is quantified by following its NIR luminescence using a liquid nitrogen-cooled Germanium photodiode. The quantum yields of $^1O_2$ produced by QD-RB and QD-Ce6 conjugates are *ca* 0.17 and *ca* 0.31, respectively. Subsequently, more efficient (*ca* 15%) production of $^1O_2$ is accomplished using conjugates of CdTe QDs and aluminium tetrasulfophthalocyanine (QD-AlSPc) [128]. Another example of QD-based $^1O_2$ production system is biocompatible and water-soluble CdSe-phorphyrin composite under two-photon excitation [129]. Here, encapsulation of QDs in micelles *via* EDC coupling without replacing the inorganic coating improved the water-solubility of QDs. The $^1O_2$ generation in this case is quantified using the disodium salt of 9,10-anthracenedipropionic acid (ADPA), which immediately reacts with $^1O_2$ and produces the endoperoxide of ADPA. The quantum

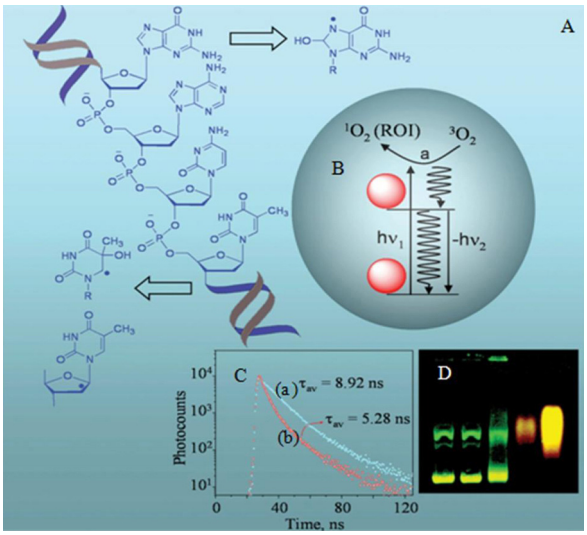

Fig. 13. (A) Guanine and thymine base damages in DNA; (B) photoactivation of a QD, various relaxation processes in a photoactivated QD, and reaction of a photoactivated QD with molecular oxygen and the formation of reactive oxygen intermediates; (C) photoluminescence decay profiles of CdSe-ZnS QDs in the presence (a) and absence (b) of oxygen; and (D) agarose gel image of plasmid DNA, photoactivated plasmid DNA, conjugates of plasmid DNA and QDs, and QDs.
Adapted with permission from [132]; the American Chemical Society.

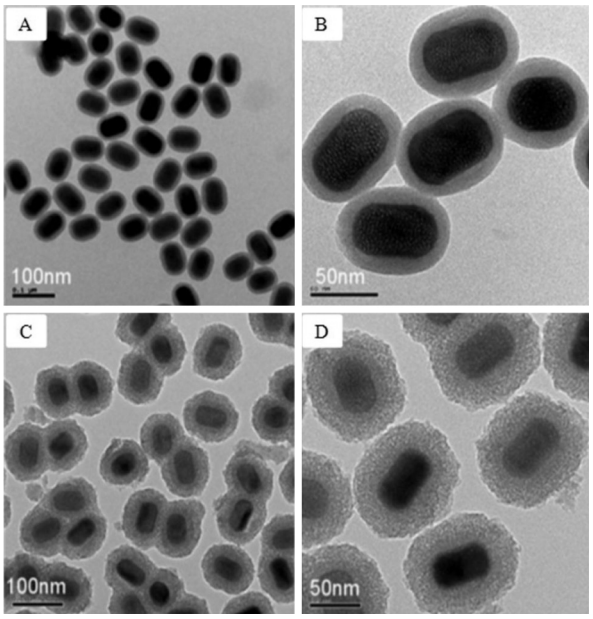

Fig. 14. TEM images of (A and B) $NaYF_4$:Yb/Er-silica NPs and (C and D) mesoporous-silica-coated $NaYF_4$:Yb/Er-silica NPs.
Adapted with permission from [142]; Wiley-VCH Verlag GmbH & Co. KGaA.

yield of the $^1O_2$ produced by the two-photon excitation is nearly twice compared to that by free porphyrin. More recently, CdTe-phthalocyanine with high triplet quantum yield (0.94) has been reported [130]. PbS QDs decorated with S-nitrosocysteine- and adsorbed on TiO_2 nanotubes is also known to produce $^1O_2$ [131]. Here, PbSe QDs are first decorated on the surface of TiO_2 nanotubes using thiolatic acid and $Pb(NO_3)_2$, and then the Pb–TiO_2 hybrid nanomaterials are functionalized with L-cysteine and loaded with NO. Subsequently, photoactivation of the hybrid system results in the release of NO and the production of $^1O_2$. The direct excitation of CdSe/ZnS QDs without the use of any PS drug is also known to produce ROI such as $^1O_2$ and hydroxyl radical and cause impairment in DNA as observed in gel electrophoresis experiments involving base-excision repair enzymes (Fig. 13) [132]. Recently, CdSe/ZnS QDs conjugated with RB is used for PDT due to its efficient production of $^1O_2$ under two-photon excitation [133]. First, the as-prepared CdSe/ZnS QDs [133–135] are phase-transferred into water using mercaptopropionic acid, and then RB molecules are conjugated to the surface of QDs *via* the EDC coupling. The $^1O_2$ production in this case is quantified using the photo-oxidation of 1,3-diphenylisobenzofuran (DPBF) into its corresponding diketonic form. HeLa cells incubated with the PS-conjugated QDs and excited using a two-photon light source show considerable decrease in their viability. Even though CdSe QDs conjugated with PS drugs are promising candidates for PDT, the toxicity of these materials limits their potentials. Recently, less toxic InP/ZnS QDs conjugated with Ce6 are used for PDT [136]. Incubation of MDA-MB-231 breast cancer cells with the InP/ZnS-Ce6 conjugate followed by UV illumination results in a decrease in the viability of the cells.

3.2. Upconversion nanoparticles (UCNPs)

UCNPs such as $NaYF_4$ doped by Er^{3+} or Yb^{3+} are synthesized by the thermal decomposition of rare-earth trifluoroacetates in the presence of a mixture of oleic acid and 1-octadecene [137]. In this synthesis, a mixture of $Ln(CF_3COOH)_3$, NaF, and oleic acid/1-octadecene is degased at 100 °C under vacuum for 1 h. The mixture is then heated rapidly to 320 °C and kept at this temperature for 30 min. UCNPs formed during this step are precipitated by the addition of ethanol followed by washing with ethanol and ultrahigh-centrifugation. Coating of UCNPs with molecules such as PEG [138] or chitosan [139] improves their water solubility and phtotostability. A simple mixing of a dispersion of UCNPs in chloroform and ploy(maleic anhydride-alt-1-octadecene)-polyethylene glycol (C18PMH-PEG) or N-succinyl-N′-octyl chitosan in water results in the formation of PEG-UCNPs [138] or chitosan modified UCNPs [139]. Common PS drugs combined with UCNPs for PDT include merocyanine-540 [140], zinc phthalocyanine (ZnPc) [141,142], Ce6 [143], or tetrasubstituted carboxy aluminum phthalocyanine (AlC_4Pc) [144]. Here, mixing of PS drugs and UCNPs in water or phosphate buffered saline (PBS) followed by the removal of unbound PS by ultrahigh centrifugation is employed for the loading of PS drugs. Core/shell mesopourous silica/$NaYF_4$ UCNPs are synthesized by two-step protocol [142] which involves the condensation of TEOS and octadecyltrimethoxysilane (C18TMS) (Fig. 14). Magnetic UCNPs ($NaGdF_4$:Yb,Er/$NaGdF_4$) are synthesized by the thermal decomposition of $NaGdF_4$:Yb/Eu and $NaGdF_4$ in a mixture of sodium trifluoroacetate, 1-octadecene, and oleic acid [145].

PDT using UCNPs is first reported for the combination of silica-coated $NaYF_4$:Er^{3+},Yb^{3+} NPs and merocyanine-540 [140]. In this case, the NPs conjugated with anti-MUC1 (episialin) are used for the targeted binding of anti-MUC1 with Episialin (MUC1) present on the surface of the cancer cells. But this method largely fails to demonstrate the activation of NPs deeply buried in tissues. ZnPc loaded $NaYF_4$:Er^{3+},Yb^{3+} NPs with organic polymer coating are also used for PDT [141]. Here, the $^1O_2$ production is quantified using ADPA sensor. Magnetic UCNPs ($NaGdF_4$:Yb, Er/$NaGdF_4$) with AlC_4Pc are also recently used for combined PDT and MR imaging [146]. Here, the $^1O_2$ production under 980 nm laser excitation in MEAR cells incubated with UCNPs results in the significant reduction of cell viability, which is determined by staining with trypan blue. PS drug-loaded silica-coated UCNPs also produce $^1O_2$ at high efficiencies and are ideal candidates for PDT [142,146]. For example, ZnPc loaded mesopourous silica-coated $NaYF_4$ UCNPs in murine bladder cancer cells produce $^1O_2$ at high efficiencies, which is monitored using a fluorescent marker, 5-(and-6)-carboxy-2′-7′-dichlorodihydrofluorescein diacetate (carboxy-H2DCFDA). Here, ROS formed by the photoactivation of ZnPc oxidize the fluorescent

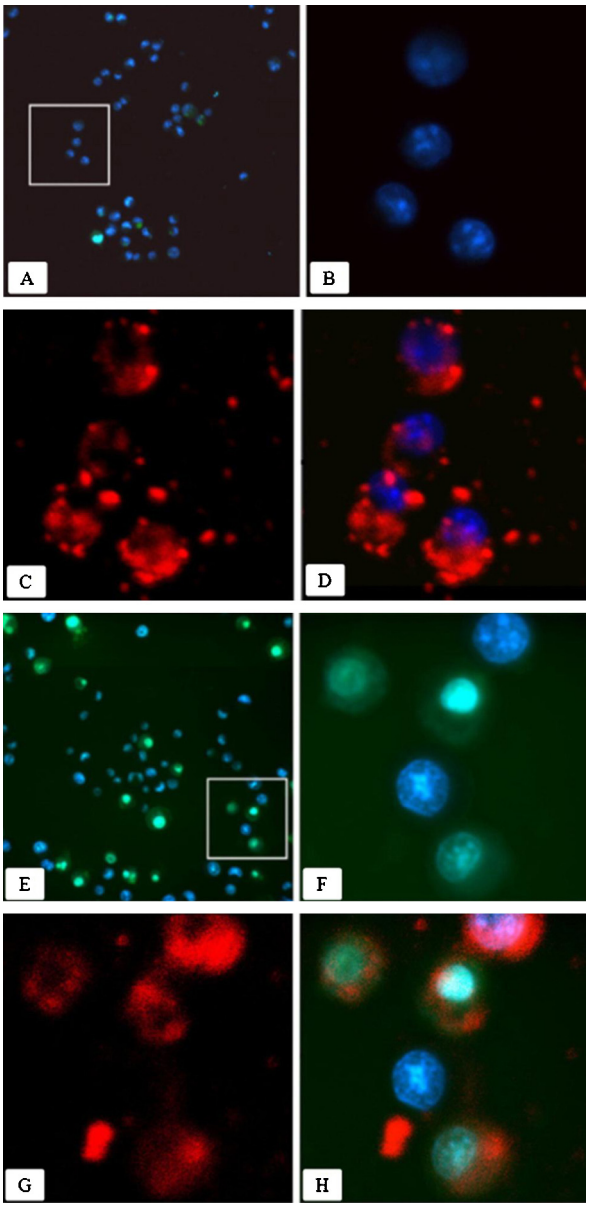

Fig. 15. Detection of oxidative stress in live cells using the Image-iT LIVE Reactive Oxygen Species (ROS) Kit. MB49-PSA cells are treated with $NaYF_4$ NPs (A–D) or ZnPc-loaded $NaYF_4$ NPs (E–H) followed by laser activation to induce oxidative stress. Cells are then labeled with carboxy-H2DCFDA, which fluoresces when oxidized in the presence of reactive oxygen species (green). Nuclei of the cells are counterstained with DAPI (blue), and the NPs are shown by their red fluorescence. Insets in (A) and (E) show the region enlarged in (B–D) and (F–H), respectively, so as to better demonstrate the more obvious changes in the cells staining pattern.
Adapted with permission from [146]; Elsevier.

marker into a bright green fluorescent product (Fig. 15). One of the key advantages of the silica-coated UCNPs is that the PS drug can be retained within the silica shell. Also, the drug can be extracted by socking the UCNPs in ethanol, which makes the NPs reusable. Many recent investigations show that UCNPs can be applied *in vivo* for PDT. For example, PDT using Ce6 loaded PEG-UCNPs in mice bearing 4T1 murine breast tumor under 980 nm laser (0.5 W cm^{-2}) excitation completely suppresses the tumor [143]. Also, the UCNPs injected during the PDT treatment are completely cleared from the body after *ca* 2 months. Chitosan-modified UCNP with ZnPc PS drug is another candidate for efficient PDT *in vivo* [139]. Here, the chitosan modification improves the dispersivity and photostability of the UCNPs and enhances the production of $^1O_2$.

3.3. Silica nanoparticles

Silica NPs encapsulated with PS have been emerged as potential PDT drugs in modern biomedical research. To-date, a wide variety of PS drugs are loaded in silica NPs, which include hypocrellin A [147,148], 2-devinyl-2-(1-hydroxyethyl)pyropheophorbide (HPPH) [149], protoporphyrin IX (PpIX) [150–152], meta-tetrahydroxyphenyl chlorin (m-THPC) [153], Pc4 [154], methylene blue [155,156], purpurin-18 [157], 2,7,12,18-tetramethyl-3,8-di(1-propoxyethyl)-13,17-bis-(3-hydroxypropyl)porphyrin (PHPP) [158], ZnPc [159], iodobenzylpyrosilane [160], pd-meso-tetra(4-carboxyphenyl) porphyrin [161], hematoporphyrin (HP) [162,163], porphyrin [164], and AlC_4Pc [165]. The best-known example of PS drug loaded in silica NPs is Foscan® which is developed by the encapsulation of meta-tetrahydroxyphenyl chlorin in silica NPs [166]. Methylene blue-incorporated silica NPs is also a promising drug in PDT [155]. However, the poor penetration ability of methylene blue into cellular compartments as well as its inactivation *via* the reduction into neutral leukomethylene blue are two major limitations. Incorporation of methylene blue in silica shell *via* Stöber method lifts these limitations. The addition of methylene blue to tetraorthosilicate during the growth of silica shell results in its trapping inside the silica matrix [156]. Silica-coated magnetic NPs are formed by the Stöber process using tetraorthosilicate [85]. Here, the magnetic core is prepared by the co-precipitation of Fe^{2+}/Fe^{3+} ions under alkaline conditions followed by the stabilization with tetraethylammonium oxide. NIR fluorescent dye (ATTO 647N) incorporated mesopourous silica NPs with palladium porphyrin (Pd-TPP) (A647@MSNPs-Pd-TPP) is synthesized starting from A647@MSNPs [167]. Here, the ATTO647N-conjugated APTMS synthesized from ATTO647N NHS ester and APTMS-EtOH is used for the synthesis of the mesoporous silica NPs (A647@MSNPs). Subsequently, Pd-TPP is covalently linked to A647@MSNPs by the reaction with silane-modified Pd-TPP. The conjugation of cRGDyK peptides on the surface of A647@MSNPs-Pd-TPP complex is found useful for the targeted delivery of the nanoparticles [167].

In contrast with silica shells, porous silica nanospheres offer better drug loading capacity, and thus more efficiency of the $^1O_2$ production. For example, HeLa cells incubated with the PS drug hypocrellin A embedded porous silica nanospheres show considerable decrease in the cell viability compared to those treated with the free PS [147]. Similarly, hypocrellin A NPs encapsulated in silica nanovehicles show higher $^1O_2$ production and active uptake into HeLa cells [148]. 2-Devinyl-2-(1-hydroxyethyl) pyropheophorbide (HPPH)-encapsulated and organically-modified silica NPs are being used in clinical trials against eosophageal cancer [151]. Protoporphyrin IX (PpIX) encapsulated in ormosil NP is another example for PS-silica NP system to show efficient $^1O_2$ production [168]. Other examples of PS drugs encapsulated in silica NPs include *m*-THPC [153], Pc4 [154], PpIX [150], HPPH [149], and methylene blue [156]. Among these NPs, HPPH-loaded and organically-modified silica NPs with covalently linked iodine produce $^1O_2$ at high efficiencies, which is due to the high triplet quantum yield contributed by the heavy atom iodine in HPPH. $^1O_2$ production by methylene blue encapsulated in phosphonate-terminated silica NPs (PSiNPs) is estimated at 0.49. The encapsulation of PpIX [151,152], iodobenzylpyrosilane [160] or phosphorescent Pd-meso-tetra(4-caroxyphenyl) porphyrin [161] in mesoporous silica matrix, or FITC-doped nonporous silica core with mesopouous silica shells containing hematoporphyrin (HP) [162] also produce $^1O_2$ at higher efficiencies. *In vitro* experiments in HeLa cells incubated with 1 mg mL^{-1} methylene blue-doped NPs show 90% decrease in the cell viability over 30 min under exposure to 635 nm laser [169]. Quadrupolar chromophores with high values of two-photon absorption cross-section incorporated in silica NPs generate $^1O_2$ at 51% efficiencies in D_2O [170]. More recently, silica-coated

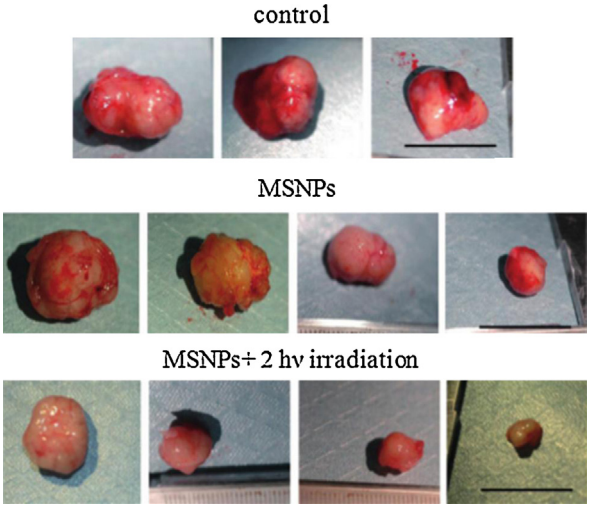

Fig. 16. The effect of two-photon excited-PDT on tumors: excised tumors from mice 30 days after treatment with saline (control), MSNPs, and a combination of MSNPs and two-photon irradiation.
Adapted with permission from [174]; Wiley-VCH Verlag GmbH & Co. KGaA.

magnetic NPs containing methylene blue [156], purpurin-18 [157], PHPP [158,171] or ZnPc [159] are exploited for the combined PDT and MRI imaging. The formation of $^1O_2$ is detected by following the characteristic luminescence band at 1270 nm. Also, a chemical method involving 1,3-diphenylisobenzofuran (DPBF) [156] and N,N-dimethyl-4-nitrosoaniline (RNO) sensors are used for the detection of $^1O_2$ [157]. ZnPc loaded Fe_3O_4-mesoporous silica NPs are also used for the delivery of the drug Ibuprofen [159]. Due to abilities to produce $^1O_2$ at high efficiencies, most of these silica NPs containing PS drugs are applied for PDT *in vitro* and *in vivo*. For example, water-soluble porphyrin-incorporated mesopourous silica NPs conjugated with mannose is used for the targeted PDT of breast cancer cells (MDA-MB-21) [164]. Other examples of PS-silica NPs for PDT include Fe_3O_4/SiO_2 core/shell nanocomposites with Ir (III) complexes [172], AlC_4Pc-loaded magnetic fluorescent Fe_3O_4/SiO_2 core/shell NPs with FA functionalization [165], Hematoporphyrin (HP)-loaded in hollow silica nanocages [163], and mesoporous silica NPs impregnated with A647@MSNPs-Pd-TPP complex [167]. As U87MG cells are incubated with A647@MSNPs-RGD-PdTPP and exposed to 532 nm laser beam (250 ± 5 mW cm^{-2}), prominent cell death is detected by PI staining of the dead cells.

PpIX-encapsulated and organically-modified silica NPs are recently used for PDT *in vivo* [150]. Biodistrubution of PpIX-silica NPs is calculated by injecting it in tumor bearing nude mice. Efficient accumulation of the NPs is accomplished in glioblastoma without any renal clearance within 24 h post injection. More recently, PpIX-loaded and organically-modified silica NPs carrying IR-820 fluorophore are used for the direct two-photon PDT and *in vivo* imaging of sentinel lymph node in mice [173]. Another example for *in vivo* PDT using silica NPs is the NIR treatment of HCT-116 xenografts in mice with porphyrin-mannose-silica NPs composite (MSNPs), which show considerable reduction in the tumor size [174]. The effect of porphyrin-mannose-silica NPs combination on tumor suppression is further evaluated *ex vivo* 30 days after the treatment (Fig. 16).

3.4. Plasmonic nanoparticles: (gold nanoparticles and gold nanorods)

Plasmonic NPs such as GNPs and GNRs find applications in PDT and PTT. The common PS drugs used in conjunction with the plasmonic NPs include phthalocyanines [175–180], toluidine blue O [181], indocyanine green [182], and $AlPcS_4$ [183]. High-quality GNPs can be synthesized by the Brust method [184]; where, the NPs are formed by the two-phase (water–toluene) reduction of $AuCl_4^-$ ions by sodium borohydride in the presence alkyl thiols. Further, the surface modifications of GNPs are carried out using PEGylation with excess HO-PEG-SH followed by the removal of excess ligand *via* ultracentrifugation [179]. A simple mixing of PS drugs with GNPs/GNRs in water results in the effective loading of the PS drug in GNPs/GNRs. Similarly, the addition of thiol functionalized phthalocyanine derivatives during the Brust synthesis results in the *in situ* formation of GNPs covalently bound with phthalocyanine derivatives [176]. Phthalocyanine-conjugated GNPs are used for the PDT of amelanotic melanoma [175] and breast cancer cells [178]. The targeted delivery of GNPs for PDT is accomplished using GNP conjugated with anti-HER2 monoclonal antibody [178]. Here, the incubation of breast cancer cells with phthalocyanine-GNPs-anti-HER2 monoclonal antibody conjugate followed by illumination with HeNe laser (632.8 nm) results in the decrease of cell viability. Similarly, the *in vivo* PDT using phthalocyanine-conjugated GNPs in C57 mice bearing amelanotic melanoma shows an extensive damage of the blood capillaries and endothelial cells [175]. Recently, a similar PDT case study has been carried out using PEG-GNP-Pc4 conjugate in tumor bearing mice, which produces $^1O_2$ at 50% efficiency in ethanol [179]. Here, the intravenous injection of the PEG-GNP-Pc4 conjugate followed by illumination with 500 nm laser shows the accumulation of Pc4 at the tumor sites within 3 h after the injection (Fig. 17). Similar to GNPs, GNRs conjugated with PS drugs also find applications in PDT [180–184]. Recently, the GNR-$AlPcS_4$ complex has been found useful for the combined PDT and PTT [183]. Here, the NIR emission of $AlPcS_4$ and its ability to produce $^1O_2$ restore when released from the complex. Thus, the fluorescence images collected from the tumor site show intense NIR fluorescence. *In vitro* studies also show that incubation of cancer cells in a solution of GNR-$AlPcS_4$ results in the efficient endocytosis of the complex, which is promising for the intracellular delivery of $AlPcS_4$.

3.5. Carbon nanomaterials

The combined PTT and PDT using carbon nanomaterials such as single walled carbon nanotube (SWCNT), multi-walled carbon nanotube (MWCNT), carbon nanohorn (CNH) and graphene oxide (GO) is practiced in combination with different PS drugs such as ZnPc [185,186], Ce6 [187,188], porphyrin [189], and pycocyanin [190]. Water solubility and biocompatibility to the carbon nanomaterials are rendered by their conjugation with different macromolecules such as bovine serum albumin (BSA) [185], aptamers [187] or chitosan [188]. Biocompatibility and water solubility to GO are rendered by PEGylation [186]. Subsequently, PS drugs are loaded onto CNT/GO by the simple mixing of CNT/GO and PS followed by the removal of excess PS by ultracentrifugation. Hydrophobic interactions between the carbon nanomaterials and the PS drugs are the keys underlying such preparations. For example, Ce6 is loaded on the surface of SWCNT by the sonication of a mixture of the two. Excess Ce6 is then filtered through a Polyvinylidene Fluoride (PVDC) membrane [188]. On the other hand, porphyrin-MWCNT (PP-MWCNT) complexes are synthesized by the carbodiimide coupling of amine-functionalized protoporphyrins with carboxylated MWCNT [189].

In vitro PDT using the BSA-ZnPc-CNH conjugate in the transformed rat fibroblasts (5RP7 cells) under 670 nm laser results in the decrease of cell viability down to 34% [187] (Fig. 18). Recently, an aptamer-Ce6-SWCNT complex has been used for the regulation of $^1O_2$ generation [187]. Here, the aptamer-Ce6 conjugates are wrapped around SWCNT (AP-SWCNT) *via* a

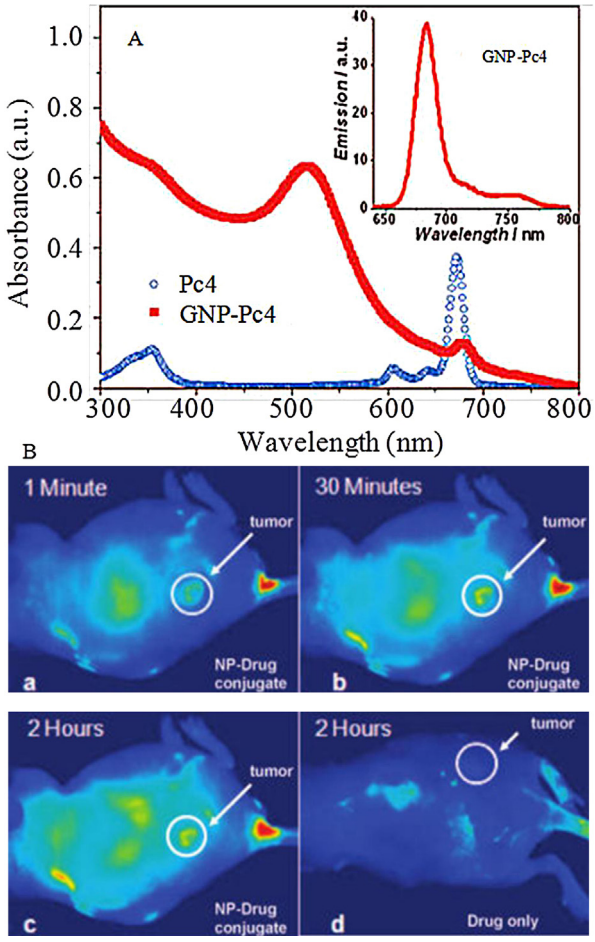

Fig. 17. (A) Absorption and emission (inset) spectra of PEG-GNP-Pc4 conjugates in normal saline. (B) Fluorescence images of a tumor-bearing mouse after being injected with PEG-GNP-Pc4 conjugates in normal saline, (a) 1 min, (b) 30 min, and (c) 120 min after intravenous tail injection. (d) Mouse injected with Pc4 alone. Adapted with permission from [179]; the American Chemical Society.

non-covalent π-stacking interaction. $^1O_2$ production is quantified using singlet oxygen sensor green (SOSG) dye. Also, Ce6-SWCNT-chitosan complex is used as a nano-PS drug for the efficient PDT of HeLa cells [188]. The 4-[3-(4-iodophenyl)-2-(4-nitrophenyl)-2H-5-tetrazolio]-1,3-benzene disulfonate (WST-1) assay of cell treated with the chitosan-ce6-SWCNT complex show considerable decrease in viability when compared with cells treated with free Ce6. Recently, PDT using PP-MWCNT complex is found to be effective for the inactivation of Influenza type A virus [189]. Here, the exceptional photostability and competent reusability of this material make it promising for the control of viral infection. MWCNT–chitosan–phycocyanin complex is also used for the growth inhibition of cancer cells *via* PDT [190]. Combined PDT and PTT are practiced *in vivo* in 5RP7 tumor-bearing mice by separately injecting the BSA-ZnPc-CNH and BSA-CNH complexes [185]. Photoactivation of the tumor milieu with 670 nm laser for 10 min after the injection results in the size-reduction of the tumor. More importantly, the tumor is completely disappeared by the combined effect of PDT and PTT.

More recently, PDT using GO-loaded with PS drugs has been reported [186,191,192]. Here, ZnPc or Ce6 is loaded on the surface of PEG functionalized GO *via* the supramolecular π stacking (Fig. 19). Even though the $^1O_2$ production by Ce6 loaded on the surface of GO is drastically suppressed by *ca* 50%, the complex is found highly effective for destroying cancer cells due to its increased cellular uptake compared with free Ce6 (Fig. 19). Here, the photothermal effect of GO under 808 nm laser is also involved in the cellular uptake of Ce6-PEG-GO.

3.6. Biodegradable polymer-based nanoparticles

Biodegradable polymer-based NPs receive remarkable attention in drug delivery due to their high capacity to carry drug molecules, ability for controlled drug delivery, versatile design, biocompatibility, and non-toxic nature [193]. The common method used for the preparation of polymer-based NPs is the emulsion polymerization or interfacial polymerization in water-in-oil or oil-in-water microemulsions. The morphology of the resulting polymer NPs is either nanospheres or core-shell NPs. The different

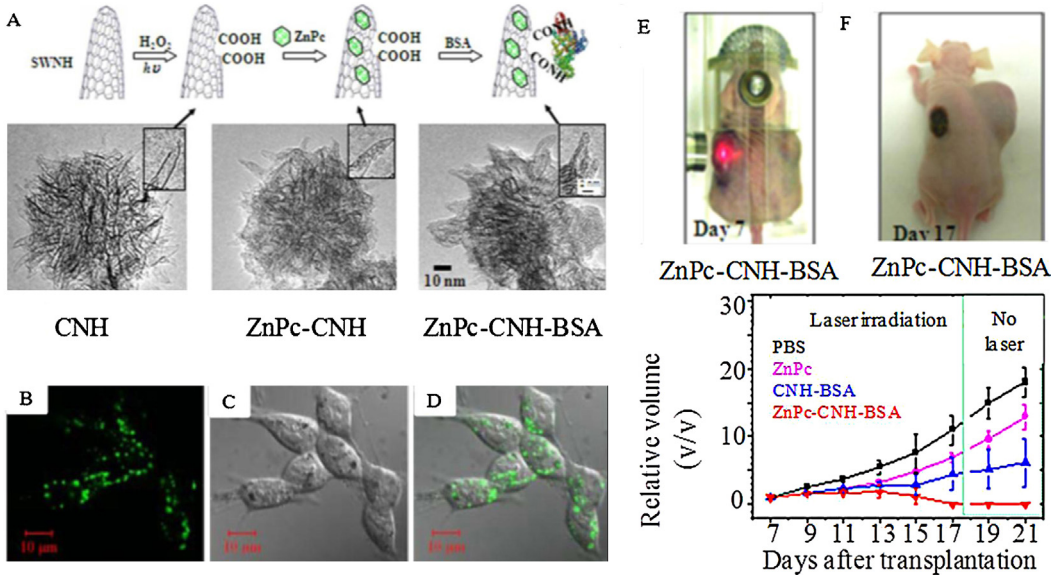

Fig. 18. (A) Preparation of ZnPc-CNH-BSA complex and TEM images of CNH derivatives. (B–D) Transformed fibroblast cells incubated with the ZnPc-CNH-BSA complex. (E, F) PD and PT destruction of tumors *in vivo*: (E) image of a mouse with large tumors on its left and right flanks 7 days after the tumor cell transplantation (the tumor on the left flank is irradiated with 670-nm laser) and (F) image of the same mouse 17 days after the treatment with the ZnPc-CNH-BSA conjugate and laser irradiation. Adapted with permission from [185]; the Natl. Acad. Sci. U. S. A.

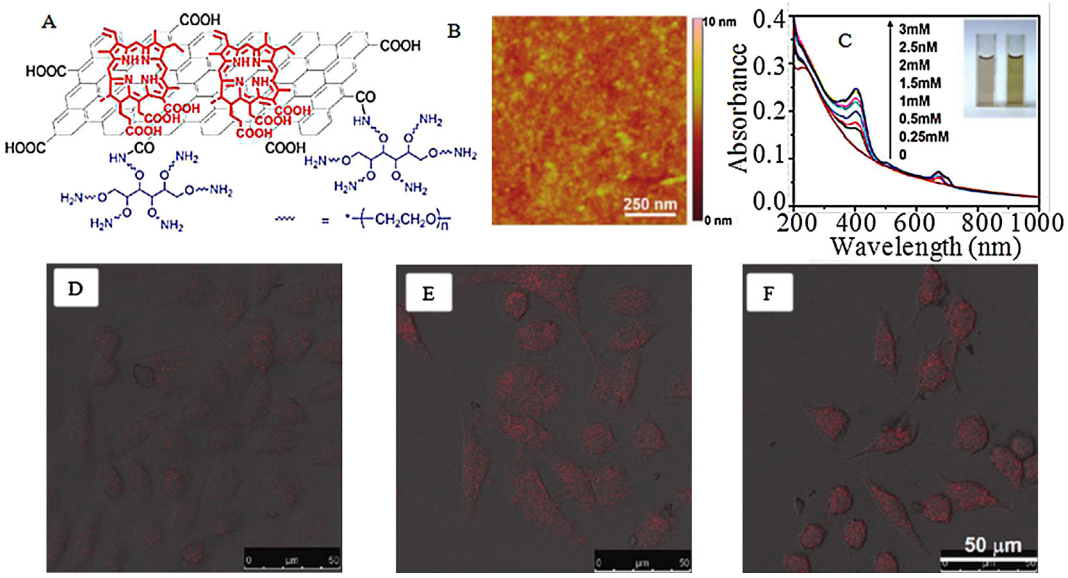

Fig. 19. (A) Scheme of Ce6 loading on GO-PEG complex. (B) AFM image of GO-PEG. (C) UV–vis absorption spectra of the GO-PEG-Ce6 conjugate at different Ce6 loading concentrations. Inset: photograph of GO-PEG (left) and GO-PEG-Ce6 (right) solutions. (D–F) Confocal images of KB cells incubated with DGO-PEG-Ce6 showing the photothermal effect on the intracellular delivery of the complex: (D) at 37 °C in dark, (E) at 37 °C under 808 nm laser irradiation (360 J cm^{-2}), and (F) at 43 °C in dark.
Adapted with permission from [186]; the American Chemical Society.

polymer-based NPs used in PDT include polystyrene spheres [194,195], PLA NPs [196], PAA NPs [197], pluronic F68 NPs [198], chitosan NPs [199–203] and hyaluronic acid NPs (HANPs) [204]. HANPs are synthesized by the chemical conjugation of aminated 5 β-cholanic acid, PEG and the black hole quencher3 to HA polymers [204]. Subsequently, Ce6 is loaded into the HANPs (Ce6-HANPs) by a simple dialysis method, which provides 80% loading efficiency. Chitosan is a linear polysaccharide molecule, composed of randomly distributed β-(1–4)-linked D-glucosamine and N-acetyl-D-glucosamine. Chitosans are widely used in biomedical applications due to their unique biocompatibility and availability of amine functionalities for chemical modifications.

The first report about biodegradable polymer NPs for PDT is on the hematoporphyrin-adsorbed polyalkylcyanoacrylate NPs for which the limitations are poor loading capacity and rapid drug release [205]. Later on, drug-loaded polymer-based NPs are conveniently adapted in PDT both *in vitro* and *in vivo* [193,206]. For example, PDT using polystyrene particles conjugated with Ce6 in human bladder carcinoma cells (MGH-U1) results in the complete destruction of tumor cells [194,195]. Another example for biodegradable polymer NPs for PDT is amine-functionalized PAA loaded with a ruthenium complex [$Ru(dpp(SO_3)_2)_3$] that produces $^1O_2$ at high quantum efficiency [197]. Here, the PAA matrix does not quench the $^1O_2$ production; however, it may be noted that the $^1O_2$ production in this case is lowered by 40% compared with that by the free dye [197]. The low efficiency of the $^1O_2$ production is due to the embedding of the sensitizer within the polymer, which in turn lowers the efficiency of energy transfer to triplet oxygen. In another case study, PDT using the lipophilic quadrupolar chromophores featuring anthracenyl- or dibromobenzene-loaded pluronic F68 NPs is evaluated in F98 cells excited with 820 nm laser [198]. The viability of the cells in this case is quantified after PDT by staining with PI and imaging under two-photon excitation. Subsequently, a high quantum efficiency of $^1O_2$ production is accomplished using polyfluorene-based NPs conjugated with tetraphenylphorphyrin [207–209]. Recent PDT investigations involving PS drugs encapsulated in chitosan-based polymer NPs show better results. Typical example is the use of protoporphyrin-conjugated glycol chitosan NPs (PpIX-GC-NPs) with cellular on/off fluorescence sensor property [199]. Here, the fluorescence of PpIX is self-quenched in the complex due to its compact structure, which disintegrates upon endocytosis and produces intense fluorescence and $^1O_2$. High efficiency of $^1O_2$ production is also accomplished for porphyrin-conjugated chitosan-based magnetic NPs [200] or Rose Bengal-grafted chitosan microcapsules [203]. These chitosan-based NPs can also be efficiently delivered in cells and proffer significant decrease in the cell viability when photoactivated.

In vivo PDT using PLA NPs conjugated with ZnPc (5 μmol kg^{-1}) in EMT-6 tumor-bearing mice shows 100% curing [191]. Ce6 loaded HANPs are also found to be ideal for *in vivo* imaging and PDT [204]. The intravenous injection of Ce6-HANPs to tumor-bearing mice results in the selective accumulation of the NPs in the tumor. Upon irradiation, Ce6 is released from the NPs, which produces $^1O_2$ as well as intense fluorescence in the tumor and results in the suppression of tumor. Highly water-soluble PpIX-GC-NPs discussed in the previous paragraph also show high tumor specificity and therapeutic efficiency when injected in SCC7 tumor-bearing mice [201,202]. In another example of PDT, porphyrin-conjugated magnetic chitosan NPs are applied *in vivo* under an external magnetic field (1 T) and NIR laser (650 nm) illumination (Fig. 20) [200]. Here, the NPs are efficiently localized in the tumor milieu under the applied magnetic field, which is detected by the T_2-weighted MR imaging. The targeted NPs are then photoactivated at 650 nm, which results in the considerable tumor regression.

3.7. Liposomes and micelles

Liposomes and micelles are artificial vehicles for the delivery of drugs and nutrients. Liposomes are composed of a lipid bilayer with an aqueous internal compartment; whereas, the micelles are closed lipid monolayers with a fatty acid core and polar surface or *vise versa*. Liposomes are widely used for the delivery of PS drugs in PDT [210–215] due to their biocompatibility, ability to protect the drugs, improve the circulatory half-life, and the release of the drugs at desired locations [214]. A variety of PS drugs are used in combination with liposomes- and micelles-based PDT. These include tetramethyl hematoporphyrin (TMHP) [216], fullerene (C_{60}/C_{70}) [217], ZnPc [218,219], Ce6 [220], benzoporphyrin

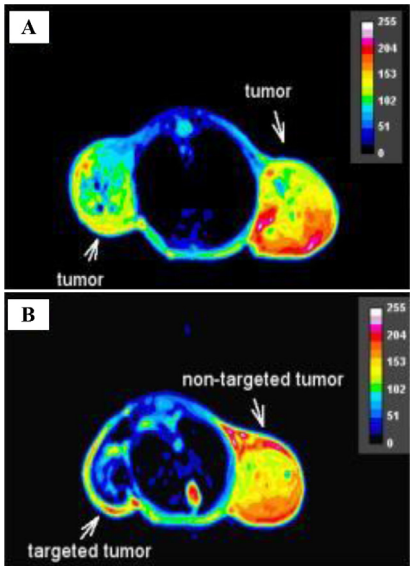

Fig. 20. T_2-weighted MR images of tumors in mice treated with porphyrin-conjugated magnetic chitosan NPs: (A) without targeting using an external magnetic field and (B) after targeting using an external magnetic field.
Adapted with permission from [200]; the IOP Science.

derivatives (BPD-MA) [221,222], pyropheophorbidemethyl ester (PPME) [223], photofrin [224,225], 2-[1-hexyloxyethyl]-2-devinylpyropheophorbide (HPPH) [226], mono-aminoporphyrin (APP) [227], and protoporphyrin IX (PpIX) [228]. There are several methods for the preparation of liposomes; for example, the dimyristoyl-L-α-phosphatidylcholine (PPME-DMPC) liposomes are prepared by the mixing of organic solutions of DMPC and PPME [223].

TMHP-incorporated unilamellar liposomes are used for PDT of human bladder carcinoma cells [216]. Water-soluble C_{60} and C_{70} incorporated in liposomes are found to be efficient PS drugs for PDT [217]. Here, the C_{70}-incorporated liposomes produce $^1O_2$ at a higher efficiency than that by C_{60}. Irradiation of micelle-like self-assembled nanospheres composed of hexa(sulfo-n-butyl)[C_{60}] fullerene (FC_4S) at 500–600 nm shows $^1O_2$ production with quantum yield up to 0.36 in water [219]. Here, photoactivation of FC_4S results in the formation of its triplet state at high efficiency and subsequent energy transfer to molecular oxygen produces single oxygen. Photofrin encapsulated liposome is another example for PDT agents [224]. First, a solution of Photofrin-encapsulated liposomes is intravenously injected into male fisher rats bearing 9L gliosarcoma. Subsequent photoactivation (632 nm and 100 mW cm^{-2}) 24 h post injection shows considerable reduction in the tumor size. On the other hand, the pentapeptide Ala-Pro-Arg-Pro-Gly-conjugated and PEGylated liposomes carrying benzoporphyrin monoacid ring A (BPD-MA) show targeted drug delivery, which is 4-fold efficient than that by PEG-liposome-BPD-MA [222]. Typical example for micelle formulation of PDT drug is APP-loaded poly(2-aminoethyl methacrylate)-polycaprolactone (PAEMA-PCL) micelles conjugated with galactosyl moiety, which is found to be ideal for the targeted PDT in human hepatocellular carcinoma (HepG2) [227]. Other examples for micelle-formulation of PS drugs include dendrimeric porphyrins and phthalocyanines, which show enhanced efficiency of PDT and reduced non-specific phototoxicity [229]. Also, recent studies show that PpIX-loaded pH-sensitive and pH-insensitive graft polymer-based micelles are ideal candidates for the photorelase of PS drugs both in *in vitro* and *in vivo* [228]. The pH-sensitive graft polymer-based micelles efficiently deliver the drug inside the cell, which makes PDT more efficient; whereas, PpIX-loaded pH-insensitive micelles are trapped within the endolysosomal bodies. Thus, the mice treated with PpIX-loaded pH-sensitive graft polymer-based micelles show a drastic decrease in the tumor size compared with the tumor in those treated with either pH-insensitive micelles or PpIX alone. Radioactive ^{131}I-labeled and ZnPc-incorporated liposomes are used for radiosyntigraphy as an early diagnostic tool and subsequent PDT [218]. Polymeric micelles of diacylphospholipid-poly-(ethylene glycol) co-loaded with Fe_3O_4 NPs and HPPH are used for the magnetically controlled drug delivery in tumor cells [226]. Here, HeLa cells treated with HPPH containing polymeric magnetic micellar dispersions are placed overnight on the top of an external magnetic field. Confocal fluorescence images from areas where the magnetic field is applied show an enhanced magnetically driven cellular uptake of the micelles, which is useful for the magnetic control of PDT.

4. Summary and perspectives

Benefitting from the recent developments in the nanomaterials field and the emergence of an interface between nanomaterials and bioconjugate chemistry, photothermal and photodynamic therapies of cancer take new dimensions in the preclinical and clinical scenario. Nanomaterials with well-defined size, shape, composition, and surface functionalities offer multimodal and multifunctional platforms for cancer management – from detection to curing both *in vitro* and *in vivo*. Strong absorption of electromagnetic radiation in the visible to NIR regions followed by the intense scattering of light or ejection of photons in the form of fluorescence makes the nanomaterials ideal for non-invasive bioimaging without engrossing any ionizing radiation. Nevertheless, additional imaging modalities can be crafted by involving nanomaterials or molecules with strong magnetic dipole-moment or radio nuclei in the nanomaterials formulations. While the photo-thermal conversion efficiencies of nanomaterials can be optimized by the tuning of their materials composition as well as size and shape, their abilities to generate reactive oxygen intermediates by the photodynamic process is either intrinsic or induced by certain photosensitizer drugs. Among the various formulations discussed in this review, nanomaterials based on gold, silica, semiconductors, polymers, and carbon show great potentials to be further formulated into photothermal and photosensitizer drugs for independent or combined photothermal and photodynamic therapies of peripheral cancers and certain infectious diseases. Some of the issues remaining in the formulation of ultimate nanomedicines for phototherapy are drug targeting and delivery, the clearance of nanomedicines or their degradation products from the body, toxicity of many components in the formulations, resources for NIR imaging and therapy, accessibility to deeply buried tumors, and information about the pharmacokinetics of the nanomedicine.

Acknowledgments

VB thank Japan Science and Technology Agency for Precursory Research for Embryonic Science and Technology (PRESTO) program and Japan Society for the Promotion of Science (JSPS) for Grant-in-Aid for Scientific Research. ESS thanks JSPS for a postdoctoral fellowship.

References

[1] X. Huang, P.K. Jain, I.H. El-Sayed, M.A. El-Sayed, Lasers Med. Sci. 23 (2008) 217.
[2] S.G. Masters, B.R. Bown, J. Cancer 8 (1992) 242.
[3] R.A. Sultan, Lasers Med. Sci. 5 (1990) 185.
[4] R.R. Anderson, J.A. Parrish, Science 220 (1983) 524.
[5] H. Chen, L. Shao, T. Ming, Z. Sun, C. Zhao, B. Yang, J. Wang, Small 6 (2010) 2272.
[6] S.K. lowers, M.A. El-Sayed, Chem. Rev. 66 (1966) 199.
[7] M.C. DeRosa, R.J. Crutchey, Coord. Chem. 223–234 (2002) 351.

[8] V. Biju, S. Mundayoor, R.V. Omkumar, A. Anas, M. Ishikawa, Biotechnol. Adv. 28 (2010) 199.
[9] J. Moan, J. Photochem. Photobiol. B: Biol. 6 (1990) 343.
[10] E. Clo, J.W. Synder, P.R. Ogilby, K.V. Gothelf, Chembiochem 8 (2007) 475.
[11] P.K. Jain, X. Huang, I.H. El-Sayed, M.A. El-Sayed, Acc. Chem. Res. 41 (2008) 1578.
[12] P.K. Jain, K.S. Lee, I.H. El-Sayed, M.A. El-Sayed, J. Phys. Chem. B 110 (2006) 7238.
[13] K.L. Kelly, E. Coronado, L.L. Zhao, G.C. Schatz, J. Phys. Chem. B 107 (2003) 668.
[14] U. Kreibig, M. Vollmer (Eds.), Optical Properties of Metal Clusters, Springer, Berlin, 1995, p. 32.
[15] S. Link, M.A. El-Sayed, Annu. Rev. Phys. Chem. 54 (2003) 331.
[16] X. Huang, I.H. El-Sayed, W. Qian, M.A. El-Sayed, J. Am. Chem. Soc. 128 (2006) 2115.
[17] S. Link, M.A. El-Sayed, Int. Rev. Phys. Chem. 19 (2000) 409.
[18] S.J. Oldenburg, R.D. Averitt, S.L. Westcott, N.J. Halas, Chem. Phys. Lett. 288 (1998) 243.
[19] C.J. Murphy, T.K. Sau, A.M. Gole, C.J. Orendorff, J. Gao, L. Gou, S.E. Hunyadi, T. Li, J. Phys. Chem. B 109 (2005) 13857.
[20] S. Link, M.B. Mohamed, M.A. El-Sayed, J. Phys. Chem. B 103 (1999) 3073.
[21] S. Link, M.B. Mohamed, M.A. El-Sayed, J. Phys. Chem. B 109 (2005) 10531.
[22] P.K. Jain, M.A. El-Sayed, Nano Lett. 7 (2007) 2854.
[23] E. Prodan, C. Radloff, N.J. Halas, P.A. Nordlander, Science 302 (2003) 419.
[24] T.S. Sreeprasad, A.K. Samal, T. Pradeep, Langmuir 23 (2007) 9463.
[25] P.R. Sajanlal, T. Pradeep, Nano Res. 2 (2009) 306.
[26] S.H. Im, Y.T. Lee, B. Wiley, Y. Xia, Angew. Chem. Int. Ed. 44 (2005) 2154.
[27] Y. Sun, Y. Xia, Science 298 (2002) 2176.
[28] Y. Sun, Y. Xia, Adv. Mater. 16 (2004) 264.
[29] C. Li, K.L. Shuford, M. Chen, E.J. Lee, S.O. Cho, ACS Nano 2 (2008) 1760.
[30] Y. Sun, Y. Xia, J. Am. Chem. Soc. 126 (2004) 3892.
[31] L. Au, Y. Chen, F. Zhou, P.H. Camargo, B. Lim, Z.Y. Li, D.S. Ginger, Y. Xia, Nano Res. 1 (2008) 441.
[32] S.K. Dondapati, T.K. Sau, C. Hrelescu, T.A. Klar, F.D. Stefani, J. Feldmann, ACS Nano 4 (2010) 6318.
[33] J. Choma, A. Dziura, D. Jamiola, P. Nyga, M. Jaroniec, Colloids Surf. A: Physicochem. Eng. Apects 373 (2011) 167.
[34] I. Washio, Y. Xiong, Y. Yin, Y. Xia, Adv. Mater. 18 (2006) 1745.
[35] C. Branca, F. Frusteri, V. Magazu, A. Mangione, J. Phys. Chem. B 108 (2004) 3469.
[36] S. Park, J. An, I. Jung, R.D. Piner, S.J. An, X. Li, A. Velamakanni, R.S. Ruoff, Nano Lett. 9 (2009) 1593.
[37] N.R. Jana, L. Gearheart, C.J. Murphy, Adv. Mater. 15 (2001) 1389.
[38] B. Nikoobakht, M.A. El-Sayed, Chem. Mater. 15 (2003) 1957.
[39] T.K. Sau, C.J. Murphy, Langmuir 20 (2004) 7414.
[40] H. Takahashi, Y. Niidome, T. Niidome, K. Kaneko, H. Kawasaki, S. Yamada, Langmuir 22 (2006) 2.
[41] T.S. Hauck, A.A. Ghazani, W.C. Chan, Small 4 (2008) 153.
[42] T. Niidome, Y. Akiyama, M. Yamagata, T. Kawano, T. Mori, Y. Niidome, Y. Katayama, J. Biomater. Sci. Polym. Ed. 20 (2009) 1203.
[43] G.V. Maltzahn, J.-H. Park, A. Agrawal, N.K. Bandaru, S.K. Das, M.J. Sailor, S.N. Bhatia, Cancer Res. 69 (2009) 3892.
[44] Z. Li, P. Huang, X. Zhang, J. Lin, S. Yang, B. Liu, F. Gao, P. Xi, Q. Ren, D. Cui, Mol. Pharma. 7 (2009) 94.
[45] J.L. Li, D. Day, M. Gu, Adv. Mater. 20 (2008) 3866.
[46] W.I. Choi, J.Y. Kim, C. Kang, C.C. Byeon, Y.H. Kim, G. Tae, ACS Nano 5 (2011) 1995.
[47] H. Ke, J. Wang, Z. Dai, Y. Jin, E. Qu, Z. Xing, C. Guo, J. Liu, X. Yue, J. Mater. Chem. 21 (2011) 5561.
[48] R. Guo, L. Zhang, H. Qian, R. Li, X. Jiang, B. Liu, Langmuir 26 (2010) 5428.
[49] D.K. Kirui, S. Krishnan, A.D. Strickland, C.A. Batt, Macromol. Biosci. 11 (2011) 779.
[50] Y.-F. Huang, K. Sefah, S. Bamrungsap, H.-T. Chang, W. Tang, Langmuir 24 (2008) 11860.
[51] D.K. Yi, I.-C. Sun, J.H. Ryu, H. Koo, C.W. Park, I.-C. Youn, K. Choi, I.C. Kwon, K. Kim, C.-H. Ahn, Bioconjug. Chem. 21 (2010) 2173.
[52] C. Wang, J. Chen, T. Talavage, J. Irudayaraj, Angew. Chem. Int. Ed. 48 (2009) 2759.
[53] E.B. Dickerson, E.C. Dreaden, X. Huang, I.V. El-Sayed, H. Chu, S. Pushpanketh, J.F. McDonald, M.A. El-Sayed, Cancer Lett. 269 (2008) 57.
[54] G. Von Maltzahn, A. Centrone, J.-H. Park, R. Ramanathan, M.J. Sailor, A. Hatton, S.N. Bhatia, Adv. Mater. 21 (2009) 3175.
[55] B.V.D. Broek, N. Devoogdt, A. D'Hollander, H.-L. Gijs, K. Jans, L. Lagae, S. Muyldermans, G. Maes, G. Borghs, ACS Nano 5 (2011) 4319.
[56] E. Ye, K.Y. Win, H.R. Tan, M. Lin, C.P. Teng, A. Mlayah, M.-Y. Han, J. Am. Chem. Soc. 133 (2011) 8506.
[57] S.A. Khan, A.K. Singh, D. Senapathi, Z. Fan, P.C. Ray, J. Mater. Chem. 21 (2011) 17705.
[58] W. Lu, A.K. Singh, S.A. Khan, D. Senapati, H. Yu, P.C. Ray, J. Am. Chem. Soc. 1332 (2010) 18103.
[59] E. Hao, R.C. Bailey, G.C. Schatz, J.T. Hupp, S. Li, Nano Lett. 4 (2004) 327.
[60] B.V. de Broek, F. Frederix, K. Bonroy, H. Jans, K. Jans, G. Borghs, G. Maes, Nanotechnology 22 (2011) 015601.
[61] S.-Y. Lin, Y.-T. Tsai, C.-C. Chen, C.-M. Lin, C.-H. Chen, J. Phys. Chem. B 108 (2000) 2134.
[62] A.K. Singh, W. Lu, D. Senapathi, S.A. Khan, Z. Fan, T. Senapathi, T. Demeritte, L. Bega, P.C. Ray, Small 7 (2011) 2517.
[63] J. Griffin, A.K. Singh, D. Senapathi, P. Rhodes, K. Mitchells, B. Robinson, E. Yu, P.C. Roy, Chem. Eur. J. 15 (2009) 342.
[64] L. Beqa, Z. Fan, A.K. Singh, D. Senapathi, P.C. Roy, ACS Appl. Mater. Interfaces 3 (2011) 3316.
[65] J. Chen, D. Wang, J. Xi, L. Au, A. Siekkinen, A. Warsen, Z.-Y. Li, H. Zhang, Y. Xia, X. Li, Nano Lett. 7 (2007) 1318.
[66] X. Wu, T. Ming, X. Wang, P. Wang, J. Wang, J. Chen, ACS Nano 4 (2010) 113.
[67] S.C. Boca, M. Potara, A.-M. Gabudean, A. Juhem, P.L. Baldeck, S. Astilean, Cancer Lett. 311 (2011) 131.
[68] M. Potara, A.M. Gabudean, S. Astilean, J. Mater. Chem. 21 (2011) 3625.
[69] L.R. Hirsch, R.J. Stafford, J.A. Bankson, S.R. Sershen, R.E. Price, J.D. Hazle, N.J. Halas, J.L. West, Proc. Natl. Acad. Sci. U. S. A. 100 (2003) 13549.
[70] V.P. Zharov, V. Galitovsky, M. Viegas, Appl. Phys. Lett. 83 (2003) 4897.
[71] M. Pitsillides, E.K. Joe, X. Wei, R.R. Anderson, C.P. Lin, Biophys. J. 84 (2003) 4023.
[72] X. Huang, W. Qian, I.H. El-Sayed, M.A. El-Sayed, Lasers Surg. Med. 39 (2007) 747.
[73] J. Nam, N. Won, H. Jin, H. Chung, S. Kim, J. Am. Chem. Soc. 131 (2009) 13639.
[74] H. Park, J. Yang, J. Lee, S. Haam, I.-H. Choi, K.-H. Yoo, ACS Nano 3 (2009) 2919.
[75] T. Nakamura, A. Tamura, H. Murotani, M. Oishi, Y. Jinji, K. Matsuishi, Y. Nagasaki, Nanoscale 2 (2010) 739.
[76] W.-S. Kuo, Y.-T. Chang, K.-C. Cho, K.-C. Chin, C.-H. Lien, C.-S. Yen, S.-J. Chen, Biomaterials 33 (2012) 3270.
[77] A.M. Elliott, R.J. Stafford, J. Schwartz, J. Wang, A.M. Shetty, C. Bourgoyne, P. ÒNeal, J. Med. Phys. 34 (2007) 3102.
[78] P. Sharma, S.C. Brown, A. Singh, N. Iwakuma, G. Pyrgiotakis, V. Krishna, J.A. Knapik, K. Barr, B.M. Moudgil, S.R. Grobmyer, J. Mater. Chem. 20 (2010) 5182.
[79] H. Liu, D. Chen, L. Li, T. Liu, L. Tan, X. Wu, F. Tang, Angew. Chem. Int. Ed. 50 (2011) 891.
[80] H. Liu, D. Chen, F. Tang, G. Du, L. Li, X. Meng, W. Liang, Y. Zhang, X. Teng, Y. Li, Nanotechnology 19 (2008) 455101.
[81] H. Ke, J. Wang, Z. Dai, Y. Jin, E. Qu, Z. Xing, C. Guo, Angew. Chem. Int. Ed. 50 (2011) 3017.
[82] J. Kim, S. Park, J.E. Lee, S.M. Jin, J.H. Lee, I.S. Lee, I. Yang, J.S. Kim, S.K. Kim, M.H. Cho, T. Hyeon, Angew. Chem. Int. Ed. 45 (2006) 7754.
[83] L. Cheng, K. Yang, Y. Li, M. Shao, S.-T. Lee, Z. Liu, Biomaterials 22 (2012) 2215.
[84] L. Cheng, K. Yang, Y. Li, J. Chen, C. Wang, M. Shao, S.-T. Lee, Z. Liu, Angew. Chem. Int. Ed. 50 (2011) 7385.
[85] W. Stöber, A. Fink, Colloid Interface Sci. 26 (1968) 62.
[86] D.P. O'Neal, L.R. Hirsch, N.J. Halas, J.D. Payne, J.L. West, Cancer Lett. 209 (2004) 171.
[87] D. Chen, L. Li, F. Tang, S. Qi, Adv. Mater. 21 (2009) 3804.
[88] Z.F. Liu, H.N. Xiao, N.J. Wisenman, J. Appl. Polym. Sci. 76 (2000) 1129.
[89] D. Niu, Y. Li, X. Qiao, L. Li, W. Zhao, H. Chen, Q. Zhao, Z. Ma, J. Shi, Chem. Commun. (2008) 4463.
[90] H. Mai, Y. Zhang, R. Si, Z. Yan, L. Sun, L. You, C. Yan, J. Am. Chem. Soc. 128 (2006) 6426.
[91] G.S. Yi, G.M. Chow, Adv. Funct. Mater. 16 (2006) 2324.
[92] F. Wang, X. Liu, J. Am. Chem. Soc. 130 (2008) 5642.
[93] H. Zhang, Y. Li, I.A. Ivanov, Y. Qu, Y. Huang, X. Duan, Angew. Chem. Int. Ed. 122 (2010) 2927.
[94] H. Zhang, Y. Li, I.A. Ivanov, Y. Qu, Y. Huang, X. Duan, Angew. Chem. Int. Ed. 49 (2010) 2865.
[95] S. Heer, K. Kompe, H.U. Gude, M. Haase, Adv. Mater. 16 (2004) 2102.
[96] A.M. Gobin, M.H. Lee, N.J. Halas, W.D. James, R.A. Drezek, J.L. West, Nano Lett. 7 (2007) 1929.
[97] E.S. Day, P.A. Thompson, L. Zhang, N.A. Lewinski, N. Ahmed, R.A. Drezek, S.M. Blaney, J.L. West, J. Neurooncol. 104 (2011) 55.
[98] A.M. Schwartzberg, T.Y. Olson, C.E. Talley, J.Z. Zhang, J. Phys. Chem B 110 (2006) 19935.
[99] W. Lu, C. Xiong, G. Zhang, Q. Huang, R. Zhang, J.Z. Zhang, C. Li, Clin. Cancer Res. 15 (2009) 876.
[100] J.Z. Zhang, J. Phys. Chem. Lett. 1 (2010) 686.
[101] M.P. Melancon, W. Lu, Z. Yang, R. Zhang, Z. Cheng, A.M. Elliot, J. Stafford, T. Olson, J.Z. Zhang, C. Li, Mol. Cancer Ther. 7 (2008) 1730.
[102] T.K. Sawyer, P.J. Sanfilippo, V.J. Hruby, M.H. Engel, C.B. Heward, J.B. Burnett, M.E. Handley, Proc. Natl. Acad. Sci. U. S. A. 77 (1980) 5754.
[103] W. Lu, M.P. Melancon, C. Xiong, Q. Hunag, A. Elliott, S. Song, R. Zhang, L.G. Flores II, J.G. Gelovani, L.V. Wang, G. Ku, R.J. Stafford, C. Li, Cancer Res. 19 (2011) 6116.
[104] M. Eghtedari, A. Oraevsky, J.A. Copland, N.A. Kotov, A. Conjusteau, M. Motamedi, Nano Lett. 7 (2007) 1914.
[105] D.R. Koenig, E.M. Weig, J.P. Kotthaus, Nat. Nanotechnol. 3 (2008) 482.
[106] F. Zhou, S. Wu, W.R. Chen, D. Xing, Small 7 (2011) 2727.
[107] K. Yang, S. Zhang, G. Zhang, X. Sun, S.-T. Lee, Z. Liu, Nano Lett. 10 (2010) 3318.
[108] F. Zhou, D. Xing, Z. Ou, B. Wu, D.E. Resasco, W.R. Chen, J. Biomed. Opt. 14 (2009) 021009.
[109] N. Huang, H. Wang, J. Zhao, H. Lui, Lasers Surg. Med. 42 (2010) 638.
[110] J.T. Robinson, S.M. Tabakman, Y. Liang, H. Wang, H.S. Casalongue, D. Vinh, H. Dai, J. Am. Chem. Soc. 133 (2011) 6825.
[111] X. Ma, H. Tao, K. Yang, L. Feng, L. Cheng, X. Shi, Y. Li, L. Guo, Z. Liu, Nano Res. 5 (2012) 199.
[112] S.-H. Hu, Y.-W. Chen, W.-T. Hunag, I.-W. Chen, S.-Y. Chen, Adv. Mater. 24 (2012) 1748.

[113] J.T. Robinson, K. Welsher, S.M. Tabakman, S.P. Sherlock, H. Wang, R. Luong, H. Dai, Nano Res. 3 (2010) 779.
[114] F. Zhou, S. Wu, S. Song, W.R. Chen, D.E. Resasco, D. Xing, Biomaterials 33 (2012) 3235.
[115] J.W. Kim, E.I. Galanzha, E.V. Shashkov, H.-M. Moon, V.P. Zharov, Nat. Nanotechnol. 4 (2009) 688.
[116] W. Zhang, Z. Guo, D. Huang, Z. Liu, H. Zhong, Biomaterials 32 (2011) 8555.
[117] C.B. Murray, D.J. Norris, M.G. Bawendi, J. Am. Chem. Soc. 115 (1993) 8706.
[118] V. Biju, T. Itoh, A. Anas, S. Sujith, M. Ishikawa, Anal. Bioanal. Chem. 391 (2008) 2469.
[119] I.L. Medintz, H.T. Uyeda, E.R. Goldman, H. Mattoussi, Nat. Mater. 4 (2005) 435.
[120] V. Biju, T. Itoh, M. Ishikawa, Chem. Soc. Rev. 39 (2010) 3031.
[121] M. Bruchez, M. Moronne, P. Gin, S. Weiss, A.P. Alivisatos, Science 281 (1998) 2013.
[122] W.C.W. Chan, S.M. Nie, Science 281 (1998) 2016.
[123] S.B. Rizvi, S. Ghaderi, M. Keshtgar, A.M. Seifalian, Nano Rev. 1 (2010) 5161.
[124] L.H. Qu, Z.A. Peng, X.G. Peng, Nano Lett. 1 (2001) 333.
[125] A.C.S. Samia, X. Chen, C. Burda, J. Am. Chem. Soc. 125 (2003) 15736.
[126] X. Chen, Y. Lou, A.C. Samiya, C. Burda, Nano Lett. 3 (2003) 799.
[127] J.M. Tsay, M. Trzoss, L. Shi, X. Kong, M. Selke, M.E. Jung, S. Weiss, J. Am. Chem. Soc. 129 (2007) 6865.
[128] J. Ma, J.Y. Chen, T. Nyokong, J. Phys. Chem. B 112 (2008) 4465.
[129] Z.-D. Qi, D.W. Li, P. Jiang, F.-L. Jiang, Y. Liu, W.-K. Wong, K.-W. Cheah, J. Mater. Chem. 21 (2011) 2455.
[130] M.E. Antunes, T. Nyokong, J. Photochem. Photobiol. A: Chem. 218 (2011) 101.
[131] C. Ratanatawante, A. Chyao, K.J. Balkus, J. Am. Chem. Soc. 133 (2011) 3492.
[132] A. Anas, H. Akita, H. Harashima, M. Ishikawa, T. Itoh, V. Biju, J. Phys. Chem. B 112 (2008) 10005.
[133] C. Fowley, N. Nomikou, A.P. McHale, P.A. McCarron, B. McCaughan, J.F. Callan, J. Mater. Chem. 22 (2012) 6456.
[134] H.Q. Nguyen, Adv. Nat. Sci. Nanosci. Nanotechnol. 1 (2010) 025004.
[135] H. Zhu, A. Prakash, D.N. Benoit, C.J. Jones, V.L. Colvin, Nanotechnology 21 (2010) 255604.
[136] G. Charron, T. Stuchinskaya, D.R. Edwards, D.A. Russell, T. Nann, J. Phys. Chem. C 116 (2012) 9334.
[137] L.A. Cheng, K. Yang, S.A. Zhang, M.W. Shao, S.T. Lee, Z.A. Liu, Nano Res. 3 (2010) 722.
[138] C. Wang, L. Cheng, Z. Liu, Biomaterials 32 (2011) 1110.
[139] S. Cui, H. Chen, H. Zhu, J. Tian, X. Chi, Z. Qian, S. Achilefu, Y. Gu, J. Mater. Chem. 22 (2012) 4861.
[140] P. Zhang, W. Steelant, M. Kumar, M. Scholfield, J. Am. Chem. Soc. 129 (2007) 4536.
[141] W. Feng, K.C. Dev, L. Zhegquan, Z. Yong, F. Xianping, W. Minquan, Nanotechnology 17 (2006) 523.
[142] H.S. Qian, H.C. Guo, P.C.-L. Ho, R. Manendran, Y. Zhang, Small 5 (2009) 2285.
[143] C. Wang, H. Tao, L. Cheng, Z. Liu, Biomaterials 32 (2011) 6145.
[144] Z. Zhao, Y. Han, C. Lin, D. Hu, F. Wang, X. Chen, Z. Chen, N. Zheng, Chem. Asian J. 7 (2012) 830.
[145] Y.I. Park, J.H. Kim, K.T. Lee, K.S. Jeon, H.B. Na, J.H. Yu, H.M. Kim, N. Lee, S.H. Choi, S.I. Baik, H. Kim, S.P. Park, B.J. Park, Y.W. Kim, S.H. Lee, S.Y. Yoon, I.C. Song, W.K. Moon, Y.D. Suh, T. Hyeon, Adv. Mater. 21 (2009) 4467.
[146] H. Guo, H. Qian, N.M. Idris, Y. Zhang, Nanomedicine 6 (2010) 486.
[147] J. Zhou, L. Zhou, C. Dong, Y. Feng, S. Wei, J. Shen, X. Wang, Mater. Lett. 62 (2008) 2910.
[148] L. Zhou, J.-H. Liu, J. Zhang, S.-H. Wei, Y.-Y. Feng, J.-H. Zhou, B.-Y. Yu, J. Shen, Int. J. Pharm. 386 (2010) 131.
[149] I. Roy, T.Y. Ohulchanskyy, H.E. Pudavar, E.J. Bergey, A.R. Oseroff, J. Morgan, T.J. Dougherty, P.N. Prasad, J. Am. Chem. Soc. 125 (2003) 7860.
[150] V. Simon, C. Devaux, A. Darmon, T. Donnet, E. Thienot, M. Germain, J. Honnorat, A. Duval, A. Pottier, E. Borghi, L. Levy, J. Marill, Photochem. Photobiol. 86 (2010) 213.
[151] L.M. Rossi, P.R. Silva, L.L.R. Vono, A.U. Ferrnandes, D.B. Tada, M.S. Baptista, Langmuir 24 (2008) 12534.
[152] B.H.-L. Tu, Y.-S. Lin, Y. Hung, L.-W. Lo, Y.-F. Chen, C.-Y. Mou, Adv. Mater. 21 (2009) 172.
[153] C. Compagnin, L. Bau, M. Mognato, L. Celotti, G. Miotto, M. Arduini, F. Moret, C. Fede, F. Selvestrel, I.M.R. Echevarria, F. mancin, E. Reddi, Nanotechnology 20 (2009) 345101.
[154] B.Z. Zhao, J.J. Yin, P.J. Bilski, C.F. Chignell, J.E. Roberts, Y.Y. He, Toxicol. Appl. Pharmacol. 241 (2009) 163.
[155] W. Tang, H. Xu, R. Kopelman, Photochem. Photobiol. 78 (2003) 587.
[156] D.B. Tada, L.L.R. Vono, E.L. Duarte, R. Itri, P.K. Kiyohara, M.S. Baptista, L.M. Rossi, Langmuir 23 (2007) 8194.
[157] F. Liu, X. Zhou, Z. Chen, P. Huang, X. Wang, Y. Zhou, Mater. Lett. 62 (2008) 2844.
[158] Z.L. Chen, Y. Sun, P. Huang, X.X. Yang, X.P. Zhou, Nanoscale Lett. 4 (2009) 400.
[159] H.J. Kim, K.J. Shin, M.K. Han, K. An, J.K. Lee, I. Honma, H. Kim, Scripta Mater. 61 (2009) 1137.
[160] T.Y. Ohulchanskyy, I. Roy, L.N. Goswami, Y. Chen, E.J. Bergey, R.K. Pandey, A.R. Oseroff, P.N. Prasad, Nano Lett. 7 (2007) 2835.
[161] S.-H. Cheng, C.-H. Lee, C.-S. Yang, F.-G. Tseng, C.-Y. Mou, L.-W. Lo, J. Mater. Chem. 19 (2009) 1252.
[162] R.R. Zhang, C.L. Wu, L.L. Tong, B. Tang, Q.H. Xu, Langmuir 25 (2009) 10153.
[163] T. Wang, L. Zhang, Z. Su, C. Wang, Y. Liao, Q. Fu, ACS Appl. Mater. Interfaces 3 (2011) 2479.
[164] D. Brevet, M. Gary-Bobo, L. Raehm, S. Richeter, O. Hocine, K. Amro, B. Loock, P. Couleaud, C. Frochot, A. Morere, P. Millard, M. Garcia, J.O. Durand, Chem. Commun. (2009) 1475.
[165] F. Wang, X. Chen, Z. Zhao, S. Tang, X. Huang, C. Lin, C. Cai, N. Zheng, J. Mater. Chem. 21 (2011) 11244.
[166] F. Yan, R. Kopelman, Phtochem. Photobiol. 78 (2003) 587.
[167] S.-H. Cheng, C.-H. Lee, M.-C. Chen, J.S. Souris, F.-G. Tseng, C.-S. Yang, C.-Y. Mou, C.-T. Chen, L.-W. Lo, J. Mater. Chem. 20 (2010) 6149.
[168] J. Qian, A. Gharibi, S. He, J. Biomed. Opt. 14 (2009) 014012.
[169] S. Kim, T.Y. Ohulchanskyy, D. Bharali, Y.H. Chen, R.K. Pandey, P.N. Prasad, J. Phys. Chem. C 113 (2009) 12641.
[170] M. Velusamy, J.Y. Shen, J.T. Lin, Y.C. Lin, C.C. Hsieh, C.H. Lai, C.W. Lai, M.L. Ho, Y.C. Chen, P.T. Chou, J.K. Hsiao, Adv. Funct. Mater. 19 (2009) 2388.
[171] F. Liu, X. Zhou, S. Ni, X. Wang, Z. Chen, Curr. Nanosci. 5 (2009) 293.
[172] C.-W. Lai, Y.-H. Wang, C.-H. Lai, M.-J. Yang, C.-Y. Chen, P.-T. Chou, C.-S. Chan, Y. Chi, Y.-C. Chen, J.-K. Hsiao, Small 4 (2008) 218.
[173] J. Qian, D. Wang, F. Cai, Q. Zhan, Y. Wang, S. He, Biomaterials 32 (2012) 4851.
[174] M.G. Bobo, Y. Mir, C. Rouxel, D. Brevet, I. Basile, M. Maynadier, P. Vaillant, O. Mongin, M.-B. Desce, A. Morere, M. Garcia, J.-O. Durad, L. Raehm, Angew. Chem. Int. Ed. 50 (2011) 11425.
[175] M. Camerin, M. Magaraggia, M. Soncin, G. Jori, M. Moreno, I. Chambrier, M.J. Cook, D.A. Russell, Eur. J. Cancer 46 (2010) 1910.
[176] D.C. Hone, P.I. Walker, R.E. Gowing, S.F. Gerland, A. Beeby, I. Chambrier, M.J. Cook, D.A. Russell, Langmuir 18 (2002) 2985.
[177] M.E. Wieder, D.C. Hone, M.J. Cook, M.M. Handsley, J. Gavrilovic, D.A. Russell, Photchem. Photobiol. Sci. 5 (2006) 727.
[178] T. Stuchinskaya, M. Moreno, M.J. Cook, D.R. Edwards, D.A. Russell, Phototchem. Photobiol. 10 (2010) 822.
[179] Y. Chen, A.N. Samia, J.D. Meyers, I. Panagopoulos, B. Fei, C. Burda, J. Am. Chem. Soc. 130 (2008) 10643.
[180] W.-S. Kuo, C.-N. Chang, Y.-T. Chang, M.-H. Yang, Y.-H. Chien, S.-Y. Chen, C.-S. Yen, Angew. Chem. Int. Ed. 49 (2010) 2711.
[181] W.-S. Kuo, C.-N. Chang, Y.-T. Chang, C.-S. Yen, Chem. Commun. (2009) 4853.
[182] L. Li, J.-Y. Chen, X. Wu, P.-N. Wang, Q. Peng, J. Phys. Chem. B 114 (2010) 17194.
[183] B. Jang, J.-Y. Park, C.-H. Tung, I.-H. Kim, Y. Choi, ACS Nano 5 (2011) 1086.
[184] M. Brust, M. Walker, D. Bethell, D.J. Schiffrin, R.J. Whymann, J. Chem. Soc. Chem. Commun. 7 (1994) 810.
[185] M. Zhang, T. Marakami, K. Ajima, K. Tsuchida, A.S.D. Sadanayaka, O. Ito, S. Iijima, M. Yudasaka, Proc. Natl. Acad. Sci. U. S. A. 105 (2008) 14773.
[186] B. Tian, C. Wang, S. Zhang, L. Feng, Z. Liu, ACS Nano 5 (2011) 7000.
[187] Z. Zhu, Z. Tang, J.A. Philips, R. Yang, H. Wang, W. Tan, J. Am. Chem. Soc. 130 (2008) 10856.
[188] H. Xiao, B. Zhu, D. Wang, Y. Pang, L. He, X. Ma, R. Wang, C. Jin, Y. Chen, X. Zhy, Carbon 50 (2012) 1681.
[189] I. Banerjee, M.P. Douaisi, D. Mondal, R.S. Kane, Nanotechnology 23 (2012) 105101.
[190] X. Liao, X. Zhang, Nanotechnology 23 (2012) 035101.
[191] D.H. Qiang, Z.Z. Lei, W.H. Yun, L.Y. Yong, G.F. Fang, S.A. Jun, P. Frank, L. Chao, S.D. Lu, Sci. China Chem. 53 (2010) 2265.
[192] P. Hunag, C. Hu, J. Lin, C. Wang, X. Wang, C. Zhang, X. Zhou, S. Guo, Theranostics 1 (2011) 240.
[193] Y.N. Konan, R. Gurny, E. Allemann, J. Photochem. Photobiol. B: Biol. 66 (2002) 89.
[194] R. Bachor, C.R. Shea, S.J. Belmonte, T. Hasan, J. Urol. 146 (1991) 1654.
[195] R. Bachor, C.R. Shea, R. Gilles, T. Hasan, Proc. Natl. Acad. Sci. U. S. A. 88 (1991) 1580.
[196] E. Allemann, N. Brasseur, O. Benrezzak, J. Rousseau, S.V. Kudrevich, R.W. Boyle, J.C. Leroux, R. Gurny, J.E. Van Lier, J. Pharm. Pharmacol. 47 (1995) 382.
[197] M.J. Moreno, E. Monson, R.G. Reddy, A. Rehemtulla, B.D. Ross, M. Philbert, R.J. Schneider, R. Kopelman, Sens. Actuat. B Chem. 90 (2003) 82.
[198] T. Gallavardin, M. maurin, S. Marotte, T. Simon, A.-M. Gabudean, Y. Bretonniere, M. Lindgren, F. Lerouge, P.L. Baldeck, O. Stephan, Y. Leverrier, J. Marvel, S. Parola, O. Maury, C. Andraud, Photochem. Photobiol. Sci. 10 (2011) 1216.
[199] S.J. Lee, H. Koo, D.-E. Lee, S. Min, S. Lee, X. Chen, Y. Choi, J.F. Leary, K. Park, S.Y. Jeong, I.C. Kwon, K. Kim, K. Choi, Biomaterials 32 (2011) 4021.
[200] Y. Sun, Z.-L. Chen, X.-X. Yang, P. Huang, X.-P. Zhou, X.-X. Du, Nanotechnology 20 (2009) 135102.
[201] S.J. Lee, K. park, Y.-K. Oh, S.-H. Kwon, S. Her, I.-S. Kim, K. Choi, S.J. Lee, H. Kim, S.G. Lee, K. Kim, I.C. Kwon, Biomaterials 30 (2009) 2929.
[202] S.J. lee, H. Koo, H. Jeong, M.S. Huh, Y. Choi, S.Y. Jeong, Y. Byun, K. Choi, K. Kim, I.C. Kwon, J. Control. Release 152 (2011) 21.
[203] X.-L. Wang, Y. Zeng, Y.-Z. Zheng, J.-F. Chen, X. Tao, L.-X. Wang, Y. Teng, Chem. Eur. J. 17 (2011) 11223.
[204] H.Y. Yoon, H. Koo, K.Y. Choi, S.J. Lee, K. Kim, I.C. Kwon, J.F. Leary, K. Park, S.H. Yuk, J.H. Park, K. Choi, Biomaterials 33 (2012) 3980.
[205] N. Brasseur, D. Brault, P. Couvreur, Int. J. Pharm. 70 (1991) 129.
[206] S. Wang, R. Gao, F. Zhou, M. Selke, J. Mater. Chem. 14 (2004) 487.
[207] L. Grimland, C. Wu, R.R. Ramoutar, J.L. Brumaghim, J. McNeill, Nanoscale 3 (2011) 1451.
[208] X. Shen, L. Li, H. Wu, S.Q. Yao, Q.-H. Xu, Nanoscale 3 (2011) 5140.
[209] X. Shen, F. He, J. Wu, G.Q. Xu, S.Q. Yao, Q.-H. Xu, Langmuir 27 (2011) 1739.
[210] D. Wohrle, M. Shopova, J.G. Moser, H. Kliesch, U. Michelsen, S. Muller, A. Weitemeyer, Macromol. Symp. 105 (1996) 127.
[211] D. Wohrle, M. Shopova, S. Muller, A.D. Milev, V.N. Mantareva, K.K. Krastev, J. Photochem. Photobio. B: Biol. 21 (1993) 155.
[212] G. Valduga, E. Reddi, S. Garbisa, G. Jori, Int. J. Cancer 75 (1998) 412.

[213] K. Ichikawa, T. Hikita, N. Maeda, Y. Takeuchi, Y. Namba, N. Oku, Biol. Pharm. Bull. 27 (2004) 443.
[214] S.K. Janardhanan, S. Narayan, G. Abbineni, A. Hayhurst, C. Mao, Mol. Cancer Ther. 9 (2010) 2524.
[215] Y. Sadzuka, F. Iwasaki, I. Sugiyama, K. Horiuchi, T. Hirano, H. Ozawa, N. Kanayama, T. Sonobe, Int. J. Pharm. 338 (2007) 306.
[216] R. Bachor, E. Reich, K. Miller, A. Ruck, Urol. Res. 23 (1995) 151.
[217] Y. Doi, A. Ikeda, M. Akiyama, M. Nagano, T. Shigematsu, T. Ogawa, T. Takeya, T. Nagasaki, Chem. Eur. J. 14 (2008) 8892.
[218] L. Polo, A. Segalla, G. Jori, G. Bocchiotti, G. Verna, R. Franceschini, R. Mooscs, P.G.D. Filippi, Cancer Lett. 109 (1996) 57.
[219] C. Yu, T. Canteenwala, M.E. El-Khouly, Y. Araki, K. Pritzker, O. Ito, B.C. Wilson, L.Y. Chiang, J. Mater. Chem. 15 (2005) 1857.
[220] Y. Namiki, T. Namiki, M. Date, K. Yanagihara, M. Yashiro, H. Takahashi, Pharmacol. Res. 50 (2004) 65.
[221] Y. Takeuchi, K. Ichikawa, S. Yonezawa, K. Kurohane, T. Koishi, M. Nanngo, Y. Manba, N. Oku, J. Control. Release 97 (2004) 231.
[222] K. Ichikawa, T. Hikita, N. Maeda, S. Yonezawa, Y. Takeuchi, T. Asai, Y. Namba, N. Oku, Biochim. Biophys. Acta 1669 (2005) 69.
[223] P.-H. Guelluy, M.-P.F. -Aupart, A. Grammenos, S. Lecart, J. Piette, M. Hoebeke, Photochem. Photobiol. Sci. 9 (2010) 1252.
[224] F. Jiang, L. Lige, J. Grenier, Y. Li, M.D. Wilson, M. Chopp, Lasers Surg. Med. 22 (1998) 74.
[225] F. Jiang, L. Lige, B. Logie, Y. Li, M. Chopp, Photochem. Photobiol. 65 (1997) 701.
[226] L.O. Cinteza, T.Y. Ohulchanskyy, Y. Sahoo, E.J. Bergey, R.K. Pandey, P.N. Prasad, Mol. Pharm. 3 (2006) 415.
[227] D.-Q. Wu, Z.-Y. Li, C. Li, J.-J. Fan, B. Lu, C. Chang, S.-X. Cheng, X.-Z. Zhang, R.-X. Zhuo, Pharm. Res. 27 (2010) 187.
[228] H.-C. Tsai, C.-H. Tsai, S.-Y. Lin, C.-R. Jhang, Y.-S. Chiang, Biomaterials 33 (2012) 1827.
[229] N. Nishiyama, Y. Morimoto, W.-D. Jang, K. kataoka, Adv. Drug Deliv. Rev. 61 (2009) 327.